Reconciling the shadow of a subduction signature with rift geochemistry and tectonic environment in Eastern Marie Byrd Land, Antarctica

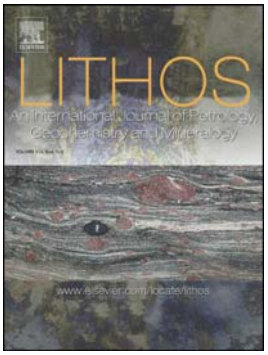

Reconciling the Shadow of a Subduction Signature with Rift Geochemistry and Tectonic Environment in Eastern Marie Byrd Land, Antarctica

Wesley E. LeMasurier, Sung Hi Choi, Stanley R. Hart, Sam Mukasa, Nick Rogers

PII: S0024-4937(16)30103-7
DOI: doi: 10.1016/j.lithos.2016.05.018
Reference: LITHOS 3936

To appear in: *LITHOS*

Received date: 20 January 2016
Accepted date: 26 May 2016

Please cite this article as: LeMasurier, Wesley E., Choi, Sung Hi, Hart, Stanley R., Mukasa, Sam, Rogers, Nick, Reconciling the Shadow of a Subduction Signature with Rift Geochemistry and Tectonic Environment in Eastern Marie Byrd Land, Antarctica, *LITHOS* (2016), doi: 10.1016/j.lithos.2016.05.018

Reconciling the Shadow of a Subduction Signature with Rift Geochemistry and Tectonic Environment in Eastern Marie Byrd Land, Antarctica.

Wesley E LeMasurier[a] Sung Hi Choi[b] Stanley R. Hart[c], Sam Mukasa[d], Nick Rogers[e]

[a]Institute of Arctic and Alpine Research, University of Colorado at Boulder, Boulder, CO, 80309-0450, USA

[b]Department of Geology and Earth Environmental Sciences, Chungnam National University, 99 Daehangno, Yuseong-gu, Daejeon 34134, South Korea.

[c]Department of Geology and Geophysics, MS 25, Woods Hole Oceanographic Institution, Woods Hole, MA 02543

[d]College of Engineering and Physical Sciences, University of New Hampshire, Durham, NH, 03824-3591, USA

[e]Department of Earth Sciences, Open University, Milton Keynes, UK

Abstract

Basalt-trachyte volcanoes in the Marie Byrd Land (MBL) Cenozoic province lie along the Amundsen Sea coast on the north flank of the West Antarctic rift. Basalts here are characterized by OIB-like geochemistry, restricted ranges of $^{87}Sr/^{86}Sr$ (0.702535 – 0.703284) and $^{143}Nd/^{144}Nd$ (0.512839–0.513008) and a wide range of $^{206}Pb/^{204}Pb$ (19.357–20.934).

Basalts at three MBL volcanoes display two anomalies compared with the above and with all other basalts in West Antarctica. They include $^{143}Nd/^{144}Nd$ (0.512778 – 0.512789) values at Mt. Takahe and Mt. Siple that are 2σ lower than other West Antarctic basalts, and Ba/Nb, Ba/La, and Ba/Th values at Mt. Murphy and Mt. Takahe that are 3-8 times higher than normal OIB. Isotope and trace element data do not support crustal and lithospheric mantle contamination, or the presence of residual mantle amphibole or phlogopite as explanations of these anomalies.

The apparent coincidence of these anomalies with the site of a pre-Cenozoic convergence zone along the Gondwanaland margin suggests a subduction influence. Major episodes of subduction and granitic plutonism took place in MBL during the Devonian, Permian, and Late Cretaceous.

Relicts in the source region, of components from these subducted slabs, provide a credible explanation for the uncoupling of Ba from other large ion lithophile elements (LILE), for its erratic distribution, and for the anomalously low $^{143}Nd/^{144}Nd$ at Mt. Takahe.

The last episode of subduction ended ~85 Ma, and was followed by continental break-up, rifting and lithospheric attenuation that produced the West Antarctic rift as we know it today. Thus, the enigmatic geochemical signatures in these three volcanoes seem to have been preserved roughly 61-85 m.y. after subduction ended. New calculations of source melting depth and a new determination of lithospheric thickness suggest that the source of the anomalies resides in a fossil mélange diapir that rose from the Cretaceous subducting slab, became attached to the base of the lithosphere at 80-100 km depth, and remained there during the subsequent plate motion and source remobilization history of this region.

Keywords. Rift volcanoes. Subduction relicts. Fossil convergent zone. Mélange diapirs.

1. Introduction

Previous research has shown that basaltic rocks across the ~3000 km length of West Antarctica (WA) (Fig. 1) display a uniformly narrow range of isotopic and trace element compositions that is unusual for a region this large (Hole and LeMasurier, 1994). For example, $^{143}Nd/^{144}Nd$ values range from 0.512839 to 0.513008 and $^{87}Sr/^{86}Sr$ from 0.702535 to 0.703520 from the tip of the Antarctic Peninsula to western Marie Byrd Land (MBL), equivalent to the distance from Anchorage to San Francisco (or Stockholm to Seville). A far greater range than this is found among basalts of the western U.S. as a whole, and even along the 800 km length of the Rio Grande Rift. Among trace elements, the uniformly narrow range is not quite so

conspicuous, but still remarkable. Trace element compositions are broadly oceanic island basalt (OIB)-like throughout WA, but high absolute values of Ba and Rb, and K/Ba<50 distinguish MBL basalts from those on the Antarctic Peninsula (Hole and LeMasurier, 1994).

In this context, we describe two volcanoes in eastern MBL, Mt. Takahe and Mt. Murphy (Fig. 1), whose Ba concentrations and $^{143}Nd/^{144}Nd$ ratios appear to set them apart from all other basalts in WA. At Mt. Takahe, $^{143}Nd/^{144}Nd$ values range from 0.512772 to 0.512790, more than 2σ below all others in WA, except for one at Mt. Siple and one in the Jones Mountains, which lie in the same zone of anomalies as Mt. Takahe and Mt. Murphy, described below. Basalts at both Mt. Takahe and Mt. Murphy are distinguishable from all other WA basalts by Ba/Th, Ba/Nb and Ba/La ratios that lie outside normal OIB ranges. Somewhat more perplexing is the fact that these anomalies lie at the east end of a geochemical gradient that extends across the province, from normal isotopic and trace element compositions in the west (e.g. Hobbs Coast, Fig. 1) to the anomalous values at Mt. Takahe and Mt. Murphy. In following the gradient still further eastward, there is also a pronounced discontinuity in Pb isotopic and trace element compositions that is apparent in crossing from MBL to the Jones Mountains in western Ellsworth Land (Hart et al., 1995).

The west-east gradient may have a paleotectonic significance. Prior to ~85 Ma, there was a convergent plate boundary along the MBL – Zealandia reconstructed continental margin, shown schematically in Fig. 2. The geochemical gradient seems to converge eastward on this fossil convergence zone, suggesting a possible subduction component to the anomalies.

In light of this background, the problems we have addressed in this study are the following. (1) Is the $^{143}Nd/^{144}Nd$ anomaly at Mt. Takahe the product of a new source, that would be virtually unique for WA basalts, or is it a result of crustal/lithospheric contamination? (2) The Ba anomaly is especially puzzling, because Ba appears to have been uncoupled from other fluid mobile elements. Is this real? Is it a product of lithospheric contamination, or the result of pre-Cenozoic subduction processes, which Plank and Langmuir (1998) have shown to be capable of uncoupling Ba from other elements? If the latter can be shown to be a reasonable possibility, what are the implications of a subduction signature lingering in the source area ~85 m.y. after subduction ended, and after the subsequent continental break-up, rifting, and lithospheric attenuation that produced the West Antarctic rift as we know it today?

2. Previous Work

The geology, petrology, and history of Mt. Takahe and Mt. Murphy volcanoes, as known before 1987, are described in the "Individual Volcano Description" sections of LeMasurier and Thomson (1990). A thorough study (by Antarctic standards) of Mt. Takahe was conducted in January 1985 when 25 localities were sampled. A total of 24 K-Ar and $^{40}Ar/^{39}Ar$ ages have now been published, none older than 192 ka (LeMasurier and Rex, 1990; Wilch et al., 1999, 2000).

Previous studies of Mt. Murphy have focused mainly on the glacial history recorded by its morphology, by tillites, pillow lavas and hyaloclastites at and near its base, and by glacial lake beds that are now 1000 m above the present ice level (Andrews and LeMasurier, 1973; LeMasurier et al., 1994; Smellie, 2001). It is also the only MBL volcano exposed, albeit

intermittently, from base to summit and has served as a model of MBL volcano structure. The generalized structure is that of a shield volcano with a basal succession of basalt, probably equal to ~90% of total volume, surmounted by a summit section of felsic and intermediate lavas. Parasitic cones of basanite follow shield building (LeMasurier, 2013). A Quaternary basalt from one of the parasitic cones has been found to be the most primitive basaltic rock in the MBL province, as measured by Mg#, Ni and Cr, and has been used to help model basalt evolution in the Executive Committee Range and the Ames and Flood Ranges (LeMasurier et al., 2003, 2011).

Geochemical studies by Futa and LeMasurier (1983), Hole and LeMasurier (1994), and Hart et al., (1997) form much of the background for this study. Futa and LeMasurier (1983) published the first set of Sr and Nd isotopic data for MBL basalts, which illustrated their OIB affinity. They also proposed the development of pockets in the mantle where metasomatizing fluids enriched the mantle source in large ion lithophile elements (LILE) and light rare earth elements (LREE), while preserving the high $^{143}Nd/^{144}Nd$ and low $^{87}Sr/^{86}Sr$ inherited from the depleted mantle source. Hole and LeMasurier (1994) presented new REE and trace element data and described the narrow range and lack of temporal change in the compositions of late Miocene and younger basalts throughout WA, suggesting they were derived from an asthenospheric source with no detectable lithospheric contamination. Hart et al., (1997) presented new Pb, Nd, and Sr isotopic data on basalts from the Hobbs Coast (Fig. 1) which demonstrated a HIMU ($^{206}Pb/^{204}Pb > 19.8$) signature, but also showed that the full range of basalts lay along a mixing line between HIMU and FOZO (focus zone; $^{206}Pb/^{204}Pb = ~19.5$) which had depth implications for this region. Modeling, using the algorithms of Herzberg and Zhang

(1996), suggested that FOZO end member basalts were produced by 3.2% melting at 110 km, and the HIMU end members by 1.6% melting at 140 km. Their study provided more evidence for a lack of contamination from ancient continental lithosphere, and noted that the mantle source was once depleted, and subsequently enriched, to account for high concentrations of the Ba to La elements, and negative slope from Nb to Lu, on chondrite-normalized spidergrams.

Wysoczanski et al., (1995), Perinelli, et al., (2011), and Martin et al., (2013) provide data on lower crustal and lithospheric mantle xenoliths from MBL and Victoria Land (Fig. 1). These data are incorporated in our isotope diagrams, and have been used to re-evaluate the possibility that the anomalies at Mt. Takahe and Mt. Murphy were produced by contamination from lower crustal and/or mantle lithospheric sources.

3. Regional Geologic Setting

Unlike the rest of the "Rim of Fire," the Pacific margin of WA is not a convergent plate boundary, but is a large intra-continental rift system within a plate that has been roughly stationary for the past 85 m.y. (Larter, et al., 2002), except for basin deepening and extension along the western Ross Sea, and possibly within the MBL interior (Cooper, et al., 1991; Cande, et al., 2000; LeMasurier, 2008). Fig. 1 shows the extent and scale of the West Antarctic rift system, and its well-defined southern boundary. In coastal MBL, clearly defined Basin and Range faulting, voluminous alkaline volcanism, and an attenuated crust, which are defining characteristics of the rift, extend to the Pacific coast, and offshore to the Marie Byrd Seamounts, suggesting that the rift has no clear northern boundary (LeMasurier and Landis, 1996; Heinemann, et al., 1999; LeMasurier, 2008).

Fig. 2 is a schematic geological reconstruction that illustrates the convergent plate margin environment that existed in coastal MBL prior to breakup of the New Zealand-Campbell Plateau block (Zealandia) from MBL, and the development of the West Antarctic rift. Forearc basin graywackes are found almost entirely in New Zealand, and the magmatic arc is represented throughout coastal WA by granitic rocks shown in the figure. These are predominantly Late Cretaceous (~90 Ma) peraluminous, calc-alkaline granites, with lesser amounts of Permian and Devonian calc-alkaline granite, representing a subduction environment that characterized this continental margin from Devonian time until subduction ceased at ~85 Ma (Larter et al., 2002); i.e. ~300 m.y. of subduction history with the convergent boundary in roughly the same position. These granitoids intrude lower Paleozoic greenschist to amphibolite facies metaclastic and metavolcanic rocks and granitic orthogneisses (Pankhurst et al., 1998; Mukasa and Dalziel, 2000). Lower crustal rocks are believed to be represented by granulite facies gabbro and norite xenoliths, and the lithospheric mantle by spinel peridotite, wehrlite, websterite and clinopyroxenite xenoliths (Wysoczanski et al., 1995).

Surface wave dispersion measurements by Ritzwoller et al., (2001) suggest a crustal thickness of 25-30 km for coastal MBL. This compares well with a more recent estimate of 22.1-32.8 km by Chaput et al., (2014). Ritzwoller et al., (2001) mapped a prominent asthenospheric anomaly between ~55 km and 200 km throughout the rift system, and they estimate a 50-60 km thickness for the lithosphere in MBL. More recently, however, An et al., (2015) used *S* velocities in the 3-D seismic model AN1-S to calculate upper mantle temperatures of the Antarctic Plate. From these results, they produce maps of the lithosphere-asthenosphere boundary depth on the basis of temperature estimations crossing the 1330°C adiabat and the

uppermost seismic low velocity zone. These maps show a lithospheric thickness of 80-100 km beneath coastal MBL.

The MBL - Zealandia breakup has most recently been estimated at 79.5 – 84 Ma (Wobbe et al., 2012). Pre-breakup rifting is recorded on land in New Zealand back to ca. 100 Ma (Bishop and Laird, 1976; LeMasurier and Landis, 1996) and back to 96 Ma on the sea floor adjacent to MBL (Wobbe et al., 2012). Most of the crustal attenuation in the rift system probably took place during this early rift episode (Lawver and Gahagan, 1994). Somewhat ambiguous sea floor data suggest subduction continued beneath eastern MBL during the interval 84 – 61 Ma, offshore of Mt. Takahe and Mt. Murphy, and is represented in the Chron 27 (61 Ma) reconstruction of Heinemann et al., (1999) by a subduction symbol.

In coastal MBL, the dominant tectonic feature within the rift is the MBL dome – a tectonomagmatic dome defined by elevations of the Late Cretaceous West Antarctic erosion surface (Fig. 1) and the focus of volcanic activity since ~28-25 Ma. Dome-centered patterns of volcanic activity suggest that the dome has risen ~100m/m.y. since the late Oligocene, accompanied throughout its history by basalt volcanism, and joined by felsic volcanism since ~19 Ma (LeMasurier and Rex, 1989; LeMasurier and Landis, 1996). As a result, the oldest felsic volcano is at the crest of the dome (Fig. 1, Mt. Flint), and the youngest, including Mt. Takahe and Mt. Siple, are along its margins. This is similar to the history of the Kenyan and Ethiopian domes in the East African rift (Baker et al., 1972; Rogers, 2006; LeMasurier, 2008).

4. Physical volcanology

Basaltic rocks appear to make up ~90% of the volume of MBL volcanoes. This is a gross estimate, based on studies of four of the 18 MBL shield volcanoes in which thick basal successions of basalt are exposed (LeMasurier, 2013). All but two of the 18 are partially buried beneath the ice sheet, exposing mainly the summit sections, which are composed of felsic and intermediate rocks and basaltic parasitic cones. These exposures create the misleading impression that MBL volcanoes are predominantly felsic. The three volcanoes described below have yielded geochemically anomalous basalt samples, and are the focus of this study.

Mt. Murphy is a late Miocene (9.3-8.2 Ma) basalt shield volcano 32 km in base diameter, with 2200 m of vertical relief (Fig. 3). It is the only MBL volcano exposed from base to summit. A 1400m basal succession of *hy-ol* basalt rests on basement rock, overlain by ~800m of trachyte and benmoreite. Samples from the southwest ridge section are all basalt, from the 500m elevation of the basement contact to the basalt/trachyte contact at 1900m, succeeded by trachyte and benmoreite flows from 1900m to 2446m (LeMasurier et al., 1994). Basanites in Table 1 were found only in parasitic cones. One $^{40}Ar/^{39}Ar$ age of 0.592 Ma (Wilch and McIntosh, 2002) is available for this latest stage of activity. Basal succession basalts appear to make up ~90% of the volcano volume (LeMasurier, 2013).

Mt. Siple is quite remote and known only from brief reconnaissance. It rises from below sea level to a 3110m summit. It was first visited in 1983. It consists of a basal succession of *hy-ol* basalt overlain by a felsic summit section. K-Ar ages of 2.0 Ma and <0.1 Ma have been obtained for basal succession sample W83-5C and parasitic cone sample W83-1 (LeMasurier and

Thomson, 1990). Trachytes, collected at the summit during a later visit, yielded an $^{40}Ar/^{39}Ar$ age of 0.227 Ma (Wilch et al., 1999). The basalt/felsic contact has not been located.

Mt. Takahe is a late Quaternary (<0.2 Ma) trachytic shield volcano ~32 km in base diameter, with 2000 m of relief above ice level (Fig. 4). It lies 200 km inland from the Amundsen Sea coast, partly buried by the West Antarctic ice sheet, which is >2 km thick at this locality (Drewry, 1983). Based on comparisons with Mt. Murphy, Mt. Siple, and two other more fully exposed volcanoes, it seems likely that the trachyte is a summit section that rests on a much larger basaltic base (LeMasurier, 2013). The exposed basaltic rocks at Mt. Takahe are basanites and hawaiites, found in parasitic cones that probably make up <1% of the exposed volume. In more fully exposed volcanoes parasitic cone basalts are geochemically similar to basal successions at Mt. Bursey and the Crary Mountains (Fig. 1), but are more silica undersaturated than the basalts exposed at the base of Mt. Murphy and Mt. Siple. The 10 analyses in Table 1 represent all accessible exposures of basaltic rock on Mt. Takahe.

5. Geochemistry

5.1 *Analytical methods*

The polar environment provides exceptionally fresh, unweathered, and unoxidized samples for analysis. This is reflected in low H_2O, CO_2, and Fe_2O_3/FeO of samples in Table 1, which are the original raw data. Glasses are fresh and unhydrated. Loss of mobile elements from devitrification is unlikely. Samples were selected for this study based on their classification as basanites, basalts and hawaiites (Fig. 5A).

Ten new major element, 21 new trace element, and 4 new isotope analyses are presented in Table 1. Major elements and originally all trace element analyses were performed by X-ray fluorescence (XRF) at the University of Nottingham (UK), except for samples 67-67A and 67-65B, which were carried out at the Washington State University Geoanalytical Lab; FeO was determined by potassium dichromate titration and F by selective ion electrode. Subsequently, five Mt. Takahe basalt samples were selected for inductively coupled mass spectrometry (ICPMS) re-analysis of 38 trace elements at the Open University (UK), following procedures described by Rogers (2006). Accuracy is generally better than 10% and often significantly better than 5%, although accuracy for a few elements lies outside these limits. Precision at the 1 sigma level is (±2%). Analysis of the standard JB-2 is included in Table 1S for inter-lab comparison with the Göttingen analyses described below.

New ICPMS trace element analyses (36 elements in Table 1) of eight Mt. Murphy samples and two Mt. Siple samples, were performed at Göttingen University. Here, 120 mg of powdered sample was reacted with 3 ml of ultra-pure HF/$HClO_4$-HF/HNO_3 mixture for 12 hours at 180°C in pressurized teflon beakers using the DAS30 Picotrace^R system at Geowissenschaftliche Zentrum University of Göttingen. Solutions were evaporated to dryness for 2 hours at 150°C. The precipitates were dissolved in 2 ml ultra-pure HNO_3, and 200 µl of a 10 ppm solution of In and Re as internal standards was added. Blanks were prepared simultaneously. The standard material JA-2 was dissolved and analyzed together with the samples, and from standard measurements the 2σ error of the method is estimated to be <20% for Nb and Ta, <10% for Be, Cs, Cu, Hf, Li, Y, Pb, Rb, Tl, Th, and U, and <10% for the rare earth

elements (REE) except for Ho, Er, Tm, Lu (<20%). ICPMS solution measurements were made on a FISONS VG PQ STE ICPMS instrument.

The four Pb isotope analyses in Table 1, and accompanying Sr and Nd isotope analyses were carried out at Woods Hole Oceanographic Institution (Mass., USA) with conventional techniques (Hauri and Hart, 1993), using sample powders which had been leached in warm 6 *N* HCL for 1 hour. Sr and Nd data carry precisions of 0.003%, and are reported relative to 0.71024 (NBS 987) and 0.511847 (La Jolla). Pb is corrected ratio by ratio for fractionation, using NBS 981 and the values given by Todt et al., (1996).

Sr and Nd isotope analysis of Mt. Takahe sample 85-19, including chemical separation and measurement was performed at the University of Michigan using VG Sector thermal ionization mass spectrometers. Analytical procedures are given in Mukasa et al., (1987, 1991). $^{87}Sr/^{86}Sr$ and $^{143}Nd/^{144}Nd$ ratios were corrected for instrumental mass fractionation by normalizing to $^{86}Sr/^{88}Sr = 0.1194$ and $^{146}Nd/^{144}Nd = 0.7219$, respectively. Replicate analyses of NBS-987 and La Jolla Nd standards gave $^{87}Sr/^{86}Sr = 0.710254 \pm 0.000011$ ($N = 30$, $2\sigma_m$) and $^{143}Nd/^{144}Nd = 0.511850 \pm 0.000019$ ($N = 30$, $2\sigma_m$).

6. Rock Compositions

6.1 *Major elements*

Major element data are presented in Table 1. In addition to Mt. Takahe and Mt. Murphy data, most of the diagrams that follow include data from 15 additional MBL localities and 6 from the Jones Mountains (Hart et al., 1995), hereafter referred to as the comparative suite

(Fig. 1 shows all localities). Geochemical characteristics of Mt. Takahe and Mt. Murphy are most distinctive and most easily interpreted in the context of the entire province. This kind of presentation also helps us evaluate whether their characteristics represent normal OIB variation, or involve other factors. Jones Mountains basalts have been well studied, and display trace element anomalies that are similar to those at Mt. Takahe and Mt. Murphy in many respects (Hart et al., 1995).

Fig. 5A presents the classification of Mt. Takahe and Mt. Murphy basaltic rocks following LeBas et al., (1986). Those at Mt. Takahe are all *ne*-normative, including basanites (*ol* >10%) and hawaiites. At Mt. Murphy, the basal succession consists of *hy-ol*- normative subalkaline basalts and alkaline basalts (*ne* = 1.04 – 1.88); parasitic cones are alkaline basalts somewhat more undersaturated than the basal succession (*ne* = 4.04 – 9.07). From only two analyses, Mt. Siple seems to resemble Mt. Murphy in that the basal succession sample is *hy-ol*- subalkaline basalt and the parasitic cone is *ne*-hawaiite (Table 1). Compared with Hawaiian basalts, all MBL samples would be considered alkali basalts (Macdonald and Katsura, 1964). Fig. 5B shows that Mt. Murphy and Mt. Siple basal successions are unusual for this province in their relatively less alkaline character, joined by only two Hobbs Coast samples, one of which is a *hy-ol* basalt at Patton Bluff (Hart et al., 1997).

Fig. 6A shows that Mt. Takahe and Mt. Murphy basaltic rocks fall into three groups. All Mt. Takahe rocks, and Mt. Murphy parasitic cones, form a high soda group, along with most other MBL basaltic rocks. The Mt. Murphy basal succession and Patton Bluff *hy-ol* basalt form a less sodic group. In addition, Mt. Murphy parasitic cones are more MgO-rich than all Mt.

Takahe basanites and most basal succession basalts. The two Mt Siple samples are intermediate in their Na_2O and MgO character.

Fig. 6B shows that the high MgO of Mt. Murphy parasitic cones and low MgO of Mt. Takahe basanites and Mt. Murphy basal succession basalts correlate closely with Ni.

Fig. 6C shows that Mt. Murphy basal successions are generally more CaO-rich than other MBL basaltic rocks. Fig. 6D plots CaO/Na_2O vs. V, both of which are sensitive to clinopyroxene (cpx) fractionation. The CaO-rich rocks can be seen to be rich in V, and have a high CaO/Na_2O ratio, suggesting that Mt. Murphy basal succession basalts have experienced less cpx fractionation than the other MBL rocks.

6.2 *Trace elements*

Trace element data are presented in Table 1 and Figs. 7, 8, 9, and 12. All diagrams that include La, Ce, Th, or Pb use ICPMS data only.

The general trace element characteristics of Mt. Takahe and Mt. Murphy are illustrated in Fig. 7 by seven samples. The most distinguishing and anomalous element is Ba. There are three high Ba and nine low-Ba samples at Mt. Murphy. The high-Ba samples are *hy-ol* basalts from localities 32 and 33 (Fig. 4; Table 1S). Low-Ba samples 32E and 33F are from the same sample sites. To illustrate the range of trace element characteristics, Fig. 7 includes hi-Ba and lo-Ba samples from Mt. Takahe (67-66B, 85-19) and Mt. Murphy (85-32B, 85-31A, 67-62), together with a representative sample from the Ames and Flood Range (AR/FR) group, which

modeling results suggest contain less than 1% crustal contamination (LeMasurier et al., 2011). Also included is a representative sample from the Jones Mountains (Hart et al., 1995).

The Ta-Nb hump and negative spikes for K and Pb are familiar OIB characteristics (Hart and Gaetani, 2006). However, both Ba and Pb characteristics are erratic, as seen by the following. The high Ba samples do not show a commensurate enrichment in other LIL elements (e.g. Rb, Th, K); but show a more negative dip in Rb and Th than the more normal AR/FR sample. Mt. Takahe sample 67-66B has the highest Pb of all seven samples and also a high Ba spike; whereas sample 19 has a moderately high Ba spike, but a large negative Pb spike. Both the high-Ba and low-Ba Mt. Murphy samples display large negative Pb spikes. The Jones Mountains sample shows low-Ba, but high-Pb. Mt. Siple and Patton Bluff *hy-ol* basalts (not shown) show neither Ba nor Pb enrichment.

Binary trace element plots are presented in Figs. 8A-F. The major observations apparent from these diagrams are (1) Ba is largely uncoupled from other LILE, (2) MBL basalts have close affinities to OIB, but with some significant deviations, and (3) there is a pronounced gradient in some trace element characteristics, from west to east, across the MBL dome among near-coastal volcanoes. The data used to position OIB mantle end members in these diagrams are found in spidergrams in Hart and Gaetani (2006), and in Tables 1S and 2S, which list data that are as yet unpublished.

Fig. 8A shows that most Mt. Takahe samples are richer in Ba than all other MBL basalts except the three hi-Ba samples from Mt Murphy, which are in a class by themselves. Conversely all the Mt. Murphy parasitic cone basalts and the lo-Ba basal succession basalts are among the

lowest Ba basaltic rocks in the province. An eastward decrease in Nb can also be seen here, and in Figs. 8B, 8D, and 8F.

Fig. 8B is intended to help visualize a contrast among the highly incompatible elements K, Nb, and Ba. In contrast to Fig. 8A, most Mt. Murphy samples, including the three high-Ba samples, plot among all other MBL basalts suggesting that Ba is uncoupled from the other LILE. Similarly, while most Mt. Takahe basaltic rocks are richer in Ba than all other MBL basalts, only two are slightly higher in K than all other MBL basalts. Fig 8C provides another example in which Ba distinguishes Mt. Takahe and Mt. Murphy basalts from others in the region.

Figure 8D is taken, in modified form, from Hole and LeMasurier (1994), with data for HIMU, EM1, EM2, and N-MORB end members from Hart and Gaetani (2006) and Table 1S. Ratios of these highly incompatible elements should not change during fractional crystallization or partial melting, and are likely to represent source characteristics. The plot shows that MBL basalts lie generally within the domain of OIB mantle end members, with the exception of the three high-Ba Mt. Murphy and most Mt. Takahe samples. All but one of the Mt. Takahe rocks are separate from the other MBL basalts and appear mildly shifted toward high Ba/Nb, higher in Ba/Nb than end member OIBs. A west to east gradient can be seen in this diagram too, in which Hobbs Coast and AR/FR volcanoes trend toward a HIMU-rich source, and Mt. Takahe to an EM-rich source.

The fields for Antarctic Peninsula and Hudson Mountains basalts, from Hole and LeMasurier (1994), show that the Mt. Takahe/Mt. Murphy Ba anomaly is truly unusual among

all West Antarctic basalts, except for those in the Hudson Mtns, which lie east of Mt. Murphy and west of the Jones Mountains (Fig. 1).

Fig. 8E presents two ratios that constrain the OIB affinities of MBL basalts. In OIB, Ba/La varies within the range 6-9, and Ba/Nb within 4-9 (Table 2). All Mt. Takahe samples lie outside these ranges, as do the three high-Ba Mt. Murphy basalts, and most AR/FR and Jones Mountains basalts. All but one Hobbs Coast and four low-Ba Mt. Murphy basalts lie within OIB boundaries. One low-Ba Mt. Murphy basalt lies barely outside these boundaries.

Fig. 8F plots two HFSE that are immobile in aqueous fluids. All MBL samples, including high-Ba and low-Ba samples, form a coherent linear trend that illustrates a constant Nb/Ta ratio for the province. It shows again the systematic eastward decrease in Nb, and also in Ta.

Two Fig. 9 diagrams explore the contrast between MBL and Jones Mountains basalts with respect to Ba and Pb. A Ce/Pb ratio >25 is a widely cited value for uncontaminated OIB (Hofmann et al., 1986); those with lower values are usually interpreted to involve crustal contamination (Hart et al., 1995). In Fig. 9A we have inverted this ratio for ease of visualization, so that indicators of a subduction influence (Ba/Nb and Pb/Ce) will rise to the right in concert. On this plot, all but one of the Mt. Takahe basaltic rocks has a Pb/Ce ratio <0.04 (equivalent to Ce/Pb>25), which implies normal OIB, but this is contradicted by Ba/Nb >9, seen here and in Fig. 8E.

All Mt. Murphy basalts lie below Pb/Ce = 0.04, along with most of the comparative suite. For Jones Mountains basalts and the one hi- Pb Mt. Takahe sample, Pb/Ce > 0.04. Thus, for Mt. Murphy, only Ba/Nb and Ba/La for the high-Ba basalts (Figs. 8C, 8D) imply significant departures

from OIB. This high Ba characteristic is shared by all Mt. Takahe basalts. By contrast, Jones Mountains basalts are the only ones that combine high Pb/Ce, with low Ba/Nb (Fig. 9A). Basalts that show the least deviation from uncontaminated OIB, in Figs. 8 and 9, are those from the Hobbs Coast, AR/FR, and Crary Mountains.

Fig. 9B shows a great deal of scatter, but is included here to emphasize the difference between MBL and Jones Mountains basalts. The plot shows significantly high Pb for Jones Mountains and the high-Pb Mt. Takahe basalt, consistent with the relations in Fig. 9A.

Fig. 9C evaluates whether variation in percent partial melting could be a factor in trace element patterns. Inspection of Table 1 shows that Nb increases with increasing silica undersaturation, i.e. with increasing normative *ne.* Thus the Nb/Y ratio has been used as an index of percent partial melting (Hole, 1988), i.e. the percent partial melting decreases with increasing Nb/Y. In this figure, the easternmost volcanic centers (Mt. Takahe, Mt. Murphy, Jones Mountains) lie at the low Nb/Y end of the array, and the westernmost centers, Hobbs Coast and AR/FR lie at the middle and high Nb/Y end. Of particular interest is the Hobbs Coast array, because the depths and percent partial melting that produced these basalts have been modeled by Hart et al., (1997). Their results show that basalts at Coleman Nunatak (Fig. 1) were formed by an estimated 1.6% melting at 140km depth, whereas the remaining basalts formed at progressively shallower depths and increasing percent melting, up to ~3.2% melting at 110 km for those at Patton and Holmes Bluffs (separate circle). The pattern in Fig. 9C conforms nicely with these conclusions, in that the Coleman basalts have the highest Nb/Y and the Holmes and Patton basalts have the lowest, among Hobbs Coast basalts.

Table 2 summarizes trace element ratios for five MBL volcanic ranges, which include 13 major shield volcanoes, and compares them with the ratios for normal OIB. At Mt. Takahe and Mt. Murphy, Ba/Nb, Ba/Th, and Ba/La ratios are 2-5 times higher than normal OIB. Ba/Th remains above normal OIB for all other MBL volcanoes, whereas Ba/Nb, Ba/La, and K/Nb are within normal OIB ranges.

7. Isotopes

Sr, Nd, and Pb isotope data for Mt. Takahe, Mt. Murphy, and Mt. Siple basaltic rocks are presented in Table 1 and Figs. 10 and 11. Although Mt. Siple trace element compositions are within the normal range for OIB (except Ba/Th), it has isotope ratios that are anomalous compared with basaltic rocks elsewhere in WA.

Fig. 10A presents Sr and Nd isotopic data in relation to the fields for MORB, HIMU, EM1, EM2 and potential MBL upper crust, lower crust, and lithospheric mantle contaminants (see Fig. 10 and 11 references). Some of the more evolved rocks are plotted here to show that Mt. Takahe basaltic rocks have more enriched Sr and Nd isotopic compositions than the mugearites, benmoreites and trachytes. The Mt. Takahe basalts cluster at the lowest $^{143}Nd/^{144}Nd$, highest $^{87}Sr/^{86}Sr$ end of the array, with $^{143}Nd/^{144}Nd$ ratios at least 2σ lower than all others, except for the Mt. Siple parasitic cone basalt and one Jones Mountains sample (see also Fig. 10C). For the province as a whole, the low $^{143}Nd/^{144}Nd$ and high $^{87}Sr/^{86}Sr$ of Mt. Takahe and Mt. Siple significantly extend the ranges of these ratios toward the EM1 end member component.

Fig. 10B, from Hole and LeMasurier (1994), illustrates the unusually narrow range for $^{143}Nd/^{144}Nd$ among basalts in WA compared with basalts from the spatially and tectonically

analogous western U.S. Subsequent (to 1994) data from MBL and Ellsworth Land do not change this picture significantly, except that the $^{143}Nd/^{144}Nd$ values reported here for Mt. Takahe basalts are 2σ lower than all other basalts in WA for which we have data. Thus, although the Mt. Takahe basalts (plus one Mt. Siple and one Jones Mountains) all lie within the $^{143}Nd/^{144}Nd$ range for OIB (Table 1S), and in that context are unremarkable, they appear to be significantly, perhaps uniquely, anomalous among basalts within the 3000 km span of WA.

Fig. 10C plots $^{143}Nd/^{144}Nd$ vs $^{87}Sr/^{86}Sr$ with the geographic localities of the source volcanoes identified (cf. Fig. 1). This plot shows a west to east gradient in isotopic composition among near coastal volcanoes. It includes data from Mt. Takahe, Mt. Murphy, and Mt. Siple, plus the comparative suite, and shows that the far western Hobbs Coast and AR/FR rocks cluster at the high $^{143}Nd/^{144}Nd$, low $^{87}Sr/^{86}Sr$ end of the array. The Mt. Murphy basalts plot at lower Nd and higher Sr isotope ratios, along with samples from the MBL dome crest (Mt. Flint and Mt. Petras) and most Jones Mountains samples. Mt. Takahe basalts cluster at the lowest $^{143}Nd/^{144}Nd$, highest $^{87}Sr/^{86}Sr$ end of the array, along with one Mt. Siple and one Jones Mountains basalt. The inland and eastern Executive Committee Range (ECR) and Crary Mountains basalts cluster with far western coastal volcanoes and do not fit the dominant pattern.

Fig. 11 shows that the full range of MBL Pb data forms an array between MORB and HIMU, with little overlap onto the fields of potential basement contaminants. It also shows how Pb data for Mt. Takahe, Mt. Murphy, and Mt. Siple compare with other volcanic centers in the province, and with the Jones Mountains. The full range of $^{206}Pb/^{204}Pb$ in MBL is 19.36 – 20.69.

Mounts Takahe, Murphy and Siple data lie well within this range (19.67-20.24). However, the $^{208}Pb/^{204}Pb$ (39.25-39.99) values extend the range toward the EM2 component. AR/FR basalts are mostly grouped on the low $^{207}Pb/^{204}Pb$ and low $^{208}Pb/^{204}Pb$ sides of the two arrays, and Mt. Takahe, Mt. Murphy and Mt. Siple basalts mainly on the high sides. Jones Mountains basalts lie nearer EM1 and further from HIMU end members than all MBL basalts.

8. **Discussion**

Major element chemistry divides Mt. Takahe, Mt. Murphy, and Mt. Siple basaltic rocks into three groups, based largely on silica saturation characteristics and percent MgO. The most likely origins of these groups do not seem relevant to understanding trace element and isotopic anomalies. It seems likely, for example, that the *hy-ol* basalts at Mt. Murphy and Mt. Siple are products of a larger percent melting, at shallower depths, than the source of the more undersaturated alkali basalts, as has been modeled for the Patton Bluff *hy-ol* basalt (Hart, et al., 1997). Most of the remaining major element characteristics of the three groups can be reasonably explained by variable fractionation of olivine, suggested by the close correlation between Ni and MgO (Fig. 6B), and to a lesser extent, clinopyroxene (Fig. 6D). Deviations from OIB and from other WA basalts are recognizable only from trace element and isotope data. The key issue is to determine whether these anomalies are related to contamination, or to source characteristics.

8.1 *The Ba anomaly*

The concentration of Ba, and the ratios Ba/Th, Ba/Nb, and Ba/La are 2-3 times higher than OIB for all but one Mt. Takahe basalt. Ba ratios among Mt. Murphy basalts are more

unusual, in that three samples are 3-8 times higher than OIB, and the remainder are among the lowest in MBL. Furthermore, both high-Ba and low-Ba samples were collected from two of the same localities (localities 32 and 33; Fig. 3, Table 1). In what follows, we attempt to test whether these values are primary magmatic characteristics, or products of post-eruptive contamination.

In addition to the usual precautions taken to collect fresh, unaltered samples and avoid lab contamination, we searched for evidence of barite contamination and could find none. Barite is a low temperature hydrothermal mineral. Its deposition would most likely be accompanied by hydrous alteration and propylitization, the latter characterized by epidote, chlorite, carbonates and albitization of feldspars. Propylitization would be obvious in the field and in thin section, and together with the negligible H_2O and CO_2 in the analyses (Table 1), we find no reason to consider the Ba anomalies as anything other than real magmatic characteristics.

The fields for potential crustal and mantle contaminants are shown in Figs. 10a and 11. The data base for the upper crust field (MBL granitoid and gneiss) is based on studies of exposed rocks (Pankhurst et al., 1998; Mukasa and Dalziel, 2000) and is quite robust. The data for lower crust and mantle fields are derived from xenolith studies and are of questionable value for interpreting source characteristics, i.e. only one sample from the cited xenolith suites contains phlogopite, the occurrence of which would strongly suggest a lithospheric mantle source. However, this sample is from Mt. Morning (Fig. 1), 1800 km west of Mt. Takahe (Martin, et al., 2013).

Contamination from the upper crust should be readily seen in isotopic compositions. The fact that Mt. Takahe basaltic rocks have more enriched Sr and Nd isotopic compositions than the mugearites, benmoreites and trachytes (Fig. 10A), and the Nb-Ta hump is within the normal range for OIB (Fig. 7), argues against basement contamination.

Mafic granulite xenoliths from the ECR (Fig. 1) (Wysoczanski et al., 1995) are believed to represent the MBL lower crust. They have more enriched Sr isotopic compositions and elevated $^{143}Nd/^{144}Nd$ ratios at a given $^{87}Sr/^{86}Sr$, as well as less radiogenic Pb isotopic compositions, compared with basalts from Mt. Takahe and Mt. Murphy.

Spinal peridotite xenoliths from Mt. Morning (Fig. 1) have been interpreted to represent lithospheric mantle (Martin et al., 2013). The available data show higher $^{143}Nd/^{144}Nd$ and less radiogenic Pb isotopic compositions than Mt. Takahe or Mt. Murphy basaltic rocks (Figs. 10a and 11). Pyroxenite xenoliths from the ECR, Mt. Morning, and Northern Victoria Land (Fig. 1) range from wehrlite to clinopyroxenite to websterite (Wysoczanski et al., 1995; Perinelli et al., 2011; Martin et al., 2013). Pyroxene-rich rocks have greater melt productivity than peridotite because of a much lower solidus (e.g. Hirschman and Stolper, 1996) and therefore could represent an enriched mantle component. Like the peridotite xenoliths, however, the pyroxenite xenoliths have elevated $^{143}Nd/^{144}Nd$ ratios at a given $^{87}Sr/^{86}Sr$, and less radiogenic Pb isotopic compositions than Mt. Takahe and Mt. Murphy basalts (Figs. 10 and 11). None of the ultramafic or lower crustal xenoliths have characteristics that constrain source depth, or that might represent contaminants that could explain the Ba and Nd isotope anomalies.

Hart et al. (1997) discuss the possibility that phlogopite and/or amphibole in the mantle lithosphere could account for the high Ba/Th of Hobbs Coast basalts, but found no clear evidence that this could be effective, without producing anomalies in other trace element ratios which we do not see. However, amphibole is a likely residual phase in the Hobbs Coast source (Hart, et al., 1997) and we have examined the possibility that pargasite in mantle lherzolite might have been a factor in producing the eastern MBL Ba anomaly. The Ba K_D for pargasite in garnet peridotite, in equilibrium with basanite liquid, is similar to that for Rb and much higher than that for Th (Adam and Green, 2011), suggesting that Th should be enriched well above Ba, and Rb enrichment should be similar to that for Ba. We do not see this in the Fig. 7 spidergrams, especially among the Ba-rich samples, i.e. there is no evidence here for an enriched lithospheric mantle source.

Finally, we observe that the east end of the trace element and isotopic gradient appears to approach the pre-Cenozoic convergence zone that existed for 300 m.y. along the reconstructed MBL-Zealandia continental margin (Fig. 2). This suggests that a subduction influence on mantle source composition should be considered. Fig. 2 is schematic, and the intersection of the gradient with the fossil convergence zone is speculative, but a similar position for the convergence zone is shown in the recently published reconstruction of Yakymchuk et al., (2015), i.e. the geographic aspect of this possibility is not unreasonable. Furthermore, Engebretson et al. (1992) estimate that up to 6 km^2 of lithosphere per km^2 of Earth surface area was subducted beneath MBL in just the past 180 m.y., which suggests that a robust source for these anomalies was at one time available.

The high Ba spike relative to other LILE (Fig. 7), and Ba/Nb >9, can be interpreted as a component of subducted sediment in the mantle source, especially in the context of the HIMU OIB signature, common to all the MBL rocks, the origin of which has been ascribed to removal of hydrous fluid and LILE from subducted slabs (Weaver, 1991). The influence of aqueous fluids is also suggested by the less coherent variation of LILE compared with HFSE (e.g. Fig. 8F vs 8B), in addition to the previously described evidence for mantle metasomatism (Futa and LeMasurier, 1983; Hart et al., 1997).

Fig. 12 compares Mt. Takahe and Mt. Murphy samples with the Ames Range, GLOSS (Plank and Langmuir, 1998) and average EM1 (Hart and Gaetani, 2006). The EM1 comparison is consistent with Figs. 8D and 10C in suggesting that EM1 is an important component in the source of the Ba-rich basalts at Mt. Takahe and Mt. Murphy. The GLOSS comparison suggests that a component of subducted sediment in the mantle source could be the source of high Ba in Mt. Murphy and Mt. Takahe basalts, and of the elevated Pb of one Mt. Takahe sample.

Plank and Langmuir (1998) provide a mechanism for uncoupling Ba from other LILE and for explaining the erratic nature of Ba distribution. They note that inconsistencies in Ba distribution can be attributed to inhomogeneities within the slab source, and also to the erratic nature of Ba transfer and subsequent emplacement in the overlying mantle wedge. For example, some diatomaceous and radiolarian oozes are rich in Ba, but some are not, and hydrothermal fluxes in the trench environment may, or may not, lead to Ba enrichment. They explain that this complex behavior leads to erratic distribution and redistribution of Ba in the subduction environment and to the uncoupling of Ba from other elements. Similarly, it has

been proposed that the distribution of Pb in oceanic crust can be influenced by hydrothermal processes (Peucker-Ehrenbrink et al., 1994; Hart et al., 1997). These relationships provide a reasonable explanation for the erratic characteristics of the Ba anomalies, via hydrous fluids removed from the slab.

8.2 *The $^{143}Nd/^{144}Nd$ anomaly at Mt. Takahe*

A comparison of Figs. 8D and 10C relates isotopic characteristics to trace element source indicators. Figs. 10A, 10C and 8D all suggest that the Mt. Takahe source is relatively rich in EM end member OIB components, whereas the Hobbs Coast and the AR/FR sources are more HIMU-rich. The slab mélange includes pelagic and terrigenous sediments that are believed to make up ~3% of the EM source (Weaver, 1991). As the term implies, they are intensely mixed along the interface between the slab and adjacent mantle wedge (e.g. Marschall and Schumacher, 2012; Vogt and Gerya, 2014). Incorporation of EM1 component, with its very low $^{143}Nd/^{144}Nd$ (Fig. 10A), provides a likely source for the Takahe isotope anomaly.

A comparison of Fig. 10C with Fig. 1 shows that the gradient toward increasing EM source components takes place generally eastward across the MBL dome. However, if the far inland ECR and Crary Mountain samples are removed, the gradient is more convincing, i.e. the ECR points should lie with the dome crest basalts, and the Crary Mtns points should lie near Takahe, based on geographic position alone (Fig. 1). This suggests that there is a coastward component as well as an eastward component to the gradient. A coastward component is to be expected if the source of the pattern is related to subduction, since Stern, et al. (1990) found that slab components in young Andean lavas decrease eastward, away from the arc. If this

eastward and coastward increase in EM components is valid, then the trend follows the eastward termination of subduction along the Pacific coast of Antarctica in Late Cretaceous time (Larter, et al., 2002). Conversely, the westward decrease of EM components toward the Hobbs Coast suggests that the zone of geochemical anomalies lies further offshore at the Hobbs Coast, and the coastline converges eastward on the zone of anomalies, just beginning to intersect them at Mt. Siple, and more centered over them at Mounts Takahe and Murphy.

In addition to the eastward gradient in Nd and Sr isotopic compositions, there is an eastward and coastward decrease in Nb (Fig. 8F). Fig. 9C (Nb/Y vs. Nb) shows an accompanying decrease in Nb/Y, which implies a general eastward increase in percent partial melting. This is supported by the gradient among Hobbs Coast samples for which source depth and percent partial melting have been modeled (Hart, et el., 1997), as described above. To extend this work to the present study, pressure and temperature estimates of melting for the five highest Mg# samples from Mt. Murphy were determined using the model of Lee et al. (2009). The five samples form a tight cluster between 1474 - 1494°C and 2.7-3.0 GPa (80-90 km depth). The lowest pressure sample is an older shield sample, whereas the other four are from younger parasitic cones (Fig. 3; Table 3S). This suggests a fairly consistent melting regime over much of the ~9 m.y. history of Mt. Murphy. It appears, therefore, that the anomaly gradient is related to an eastward increase in EM components, an increase in percent partial melting, and a decrease in source depth, all of which accompany the tapping of a source that contains progressively more remnants of the pre-Cenozoic subduction mélange.

There is a remarkable coincidence between this new calculation of source melting depth, at 80-90 km, and the newly published seismic data (An et al., 2015) which indicate an 80-100 km lithospheric thickness beneath MBL. These suggest that the Mt. Murphy and Mt. Takahe source lay at the base of the lithosphere. This source region was apparently impregnated by aqueous fluids and sedimentary components derived from Cretaceous, or conceivably older, slabs.

If this interpretation is approximately correct, then these geochemical relicts have persisted in the mantle source for as much as 85 m.y. after subduction ended. Although it is well established that de-watering of subducted slabs metasomatizes the overlying mantle wedge, there is still uncertainty about how long the signature of this process remains in the mantle wedge after subduction ends. Farmer et al., (2013) found that the metasomatized mantle wedge in the northern Sierra Nevada (California) was not involved in any post-subduction magmatism. At the other extreme, Pegram (1990) argued that the Mesozoic rift tholeiites of the eastern U.S. were derived from mantle that was impacted by Grenvillian (1 Ga) subduction. Closer to the subject of this paper, late Miocene basalts in the Jones Mountains display low Ce/Pb ratios (8.5-17.6), low $^{207}Pb/^{204}Pb$, and high Pb/Pb*, that have been interpreted by Hart et al., (1995) as the mark of subduction impregnated subcontinental lithosphere that has remained in the source area roughly 50-60 m.y. after subduction ended in this region. Thus, the suggestion that a subduction signature remains ~85 m.y. after subduction ended in MBL is not without precedent.

8.3 *The Ba-Pb discontinuity*

Although some aspects of the west – east geochemical gradient continue smoothly from Mt. Murphy to the Jones Mountains (e.g. Nb), there is an abrupt discontinuity in Ba and Pb trace element and isotopic anomalies between the two. High Ba/Nb, and Ba/La distinguish Mt. Takahe and Mt. Murphy basalts from the Jones Mountains and the rest of MBL (Table 2, Figs. 8C, D, E), whereas high Pb/Ce and low Th/Pb separate the Jones Mountains from all MBL (Figs. 9B, D). Similarly, low $^{143}Nd/^{144}Nd$, coupled with low $^{87}Sr/^{86}Sr$ at a given $^{143}Nd/^{144}Nd$ (Fig. 10B), distinguishes Mt. Takahe from the Jones Mountains and all other MBL volcanoes, whereas low $^{206}Pb/^{204}Pb$ separates the Jones Mountains from all MBL (Fig. 11).

The area of this discontinuity (~100^{o} W) lies near the Late Cretaceous/ early Cenozoic boundary between the Antarctic plate and the Phoenix plate (Eagles et al., 2004 ; Larter et al., 2002), which was a complex zone of rapidly changing plate boundaries at that time. Larter et al., (2002) show that subduction continued from Thurston Island (Fig. 1) eastward at least until 45 Ma, long after it had stopped farther to the west. Plank and Langmuir (1998) have found that there is no common stratigraphy among trench sections. Each subduction environment is characterized by a different sedimentary package. This must certainly have been the case where subduction ended adjacent to MBL at ~85 Ma, but continued perhaps as much as 40 m.y. longer off the coast of the Jones Mountains. We have no data on the composition of trench sediments in either of these environments, but it seems reasonable to speculate that they were different from each other, and that this resulted in different subduction signatures for MBL compared to the Jones Mountains.

8.4 *Implications for mantle dynamics*

The preceding discussion has led us to propose that processes operating within a subduction environment provide the most reasonable explanations for (1) the high – Ba anomalies, (2) their uncoupling from other LILE, (3) the anomalously low $^{143}Nd/^{144}Nd$ at Mt. Takahe, and (4) the eastward and coastward gradient of anomalies across the province. In this context, the Marschall and Schumacher (2012) mélange–diaper model of the subduction environment provides a unifying conceptual framework that embraces the processes interpreted above.

The key elements to the model involve the development of instabilities along the slab mantle interface during subduction, and consequent rise of mélange diapirs into the mantle wedge. During their rise, these materials are heated, cross the dehydration curves for serpentine and chlorite yielding hydrous fluids, and are partially melted yielding arc volcanism and, in MBL, the Cretaceous calc-alkaline granitoids.

The new lithospheric thickness data, the calculated depth of melting beneath Mt. Murphy, and the anomalies themselves, suggest that the remains of such a diaper are now attached to the base of the MBL lithosphere and were remobilized during late Cenozoic volcanism. The long term preservation of the subduction signatures (i.e. the anomalies) suggests that the source materials remained attached to the base of the lithosphere during any subsequent motion of the plate.

9. Summary and Conclusions

1. Basaltic rocks at Mt. Takahe and Mt. Murphy volcanoes display anomalies in Ba/Nb, Ba/La and Ba/Th that are well outside normal OIB ranges, and outside the ranges for basaltic rocks anywhere else in West Antarctica, except the Hudson Mtns.

2. Basaltic rocks at Mt.Takahe and Mt. Siple volcanoes display $^{143}Nd/^{144}Nd$ ratios that, although within the range for normal OIB, are 2σ below all other basaltic rocks in WA.

3. Isotopic and trace element data do not support crustal or lithospheric mantle contamination, or residual phlogopite or pargasite in the mantle source, as viable explanations for these anomalies. No other probable high-Ba, low radiogenic Nd lithospheric source has yet been reported from MBL.

4. There is a geochemical gradient in MBL, characterized by eastward and coastward decreasing $^{143}Nd/^{144}Nd$, increasing $^{87}Sr/^{86}Sr_i$ and decreasing Nb and Ta. These gradients appear to gradually intersect the position of the convergence zone that lay seaward of the reconstructed MBL-Zealandia continental margin in pre-Cenozoic time. The pattern of anomalies suggests that the paleo-convergence zone lies offshore of western MBL and onshore in eastern MBL. This led to our interpretation that the Ba anomaly, and the Nd and Sr isotopic anomalies, are the product of residual subduction components in the mantle source.

5. The high-Ba anomalies, uncoupling of Ba from other LILE, and the erratic nature of the anomalies are most easily explained by some combination of hydrothermal activity, removal and uncoupling of Ba from the subduction mélange during slab de-watering, and

subsequent hydrous fluid transfer. Subsequent rise of hydrous fluids resulted in erratic, and often independent, Ba enrichment of mantle source rocks.

6. The low $^{143}Nd/^{144}Nd$ of Mt. Takahe (and one Mt. Siple) basaltic rocks are best explained by partial melting of slab mélange sediments in the mantle source that were richer in EM components than the sources of other MBL volcanoes.

7. Although Mt. Takahe, Mt. Murphy, Mt. Siple volcanoes, and the Jones Mountains, all display relict subduction signatures that seem related to the same convergent margin, the predominantly Pb-related anomalies in the Jones Mountains (high Pb/Ce, low $^{206}Pb/^{204}Pb$) are conspicuously different from the high-Ba and low $^{143}Nd/^{144}Nd$ anomalies that characterize the eastern, coastal MBL volcanoes. The geochemical discontinuity between the two regions coincides roughly with a tectonic boundary in the sea floor between the MBL sector, where subduction ceased ~85 Ma, and the Ellsworth Land sector, where subduction ended ~45 Ma. We speculate that a likely source of the discontinuity lies with differences in the composition of subducted sediments between the two regions.

8. We present new calculations that suggest a source melting depth of 80-90 km beneath Mt. Murphy. This roughly coincides with the base of the lithosphere, which was recently determined to be 80-100 km thick in MBL. We propose that the source of the anomalies resides with a fossil mélange diapir that rose from the Cretaceous subducting slab and became attached to the base of the lithosphere, where it remained during subsequent plate motions and Late Cenozoic remobilization, thereby preserving the subduction signature.

Acknowledgements

Work on the geochemistry of Marie Byrd Land volcanoes has been supported by NSF Grants #0536526 (to WEL) and #9419094 (to SRH) administered by the Office of Polar Programs. WEL thanks the Institute of Arctic and Alpine Research (INSTAAR) for funds to cover publication costs. Lang Farmer and Chuck Stern, provided helpful comments and advice regarding the potential residence times of subduction signatures. Steve Cande guided us skillfully through the intricacies of Cretaceous/Cenozoic sea floor tectonics of the Amundsen Sea region. Gerhard Wörner provided 10 new ICPMS analyses of Mt. Murphy and Mt. Siple samples, and comprehensive reviews of early drafts. Rob Larter and Graeme Eagles provided invaluable help with lithospheric thickness in MBL and the history of plate motions over the past 100 m.y. We are pleased to acknowledge interesting and constructive formal reviews by Godfrey Fitton and Adam Martin which greatly improved our interpretations.

References

Adam, J., Green, T., 2011. Trace element partitioning between mica- and amphibole-bearing garnet lherzolite and hydrous basanite melt: 2. Tasmanian Cainozoic basalts and the origins of intraplate basaltic magmas. Contributions to Mineralogy and Petrology, 161, 883-899.

An, M., Wiens, D.A., Zhao, Y., Feng, M., Nyblade, A., Kanao, M., Li, Y., Maggi, A., Lévêque, J.-J., 2015. Temperature, lithosphere-asthenosphere boundary, and heat flux beneath the Antarctic Plate inferred from seismic velocities. Journal of Geophysical Research 120, 8720-8742, doi: 10.1002/2015JB011917.

Andrews, J.T., LeMasurier, W.E., 1973. Rates of Quaternary glacial erosion and corrie formation, Marie Byrd Land, Antarctica. Geology 1, 75-80.

Baker, B.H., Mohr, P.A., Williams, L.A.J., 1972. Geology of the Eastern Rift System of Africa. Geological Society of America Special Paper 136, 67p.

Bishop, D.G., Laird, M.G., 1976. Stratigraphy and depositional environment of the Kyeburn Formation (Cretaceous), a wedge of coarse terrestrial sediments in Central Otago. Royal Society of New Zealand Journal 6, 55-71.

Cande, S.C., Stock, J.M., Müller, R.D., Ishihara, T., 2000. Cenozoic motion between East and West Antarctica. Nature 404, 145-150.

Chaput, J., Aster, R.C., Huerta, A., Sun, X., Lloyd, A., Wiens, D., Nyblade, A., Anandakrishnan, S., Winberry, J.P., Wilson, T., 2014. The crustal thickness of West Antarctica. Journal of Geophysical Research Solid Earth 119, 1-18, doi: 10.1002/2013JB010642.

Cooper, A.K., Davey, F.J., Hinz, K., 1991. Crustal extension and origin of sedimentary basins beneath the Ross Sea and Ross Ice Shelf, Antarctica, in: Thomson, M.R.A., Crame, J.A., Thomson, J.W. (Eds.) The geological evolution of Antarctica. Cambridge University Press, Cambridge, pp 285-291.

Cooper, R.A., Landis, C.A., LeMasurier, W.E., Speden, I.G., 1982. Geologic history and regional patterns in New Zealand and West Antarctica – Their paleotectonic and paleogeographic significance, in: Craddock, C. (Ed.) Antarctic geoscience, University of Wisconsin Press, Madison, pp 43-53

Drewry, D.J. 1983. Antarctica: glaciological and geophysical folio. Scott Polar Research Institute, University of Cambridge, Cambridge, 9 sheets

Eagles, G., Gohl, K., Larter, R.D., 2004. High-resolution animated tectonic reconstruction of the South Pacific and West Antarctic Margin. Geochemistry, Geophysics, Geosystems 5, Q07002, doi:10.1029/2003GC000657.

Engebretson, D.C., Kelley, K.P., Cashman, H.J., 1992. 180 Million Years of subduction. GSA Today 2, 93-100.

Farmer, G.L., Glazner, A.F., Kortemeier, W.T., Cosca, M.A., Jones, C.H., Moore, J.E., Schweickert, R.A., 2013. Mantle lithosphere as a source of postsubduction magmatism, northern Sierra Nevada, California. Geosphere 9, 1-22. Doi: 10.1130/GES00885.1

Fitton, J.G., James, D., Kempton, P.D., Ormerod, D.S., and Leeman, W.P., 1988. The role of lithospheric mantle in the generation of late Cenozoic magmas in the Western United States, in: Menzies, M.A., Cox, K.G. (Eds), Oceanic and continental lithosphere. Journal of Petrology Special Lithosphere Issue, pp. 331-349.

Futa, K., LeMasurier, W.E., 1983. Nd and Sr isotopic studies on Cenozoic mafic lavas from West Antarctica: another source for continental alkali basalts. Contributions to Mineralogy and Petrology 83, 38-44

Hart, S.R., 1984. A large-scale isotope anomaly in the Southern Hemisphere mantle. Nature 309, 753-757.

Hart, S.R., Blusztajn, J., LeMasurier, W.E., Rex, D.C., 1997. Hobbs Coast Cenozoic volcanism: Implications for the West Antarctic rift system. Chemical Geology 139, 223-248.

Hart, S.R., Blusztajn, J., Craddock, C., 1995. Cenozoic volcanism in Antarctica: Jones Mountains and Peter I Island. Geochimica et Cosmochimica Acta 59, 3379-3388

Hart, S.R., Gaetani, G.A., 2006. Mantle Pb paradoxes: the sulfide solution. Contributions to Mineralogy and Petrology 152, 295-308

Hauri, E.H., Hart, S.R., 1993. Re-Os isotope systematics of HIMU and EMII oceanic island basalts from the South Pacific Ocean. Earth and Planetary Science Letters 114, 353-371.

Heinemann, J., Stock, J., Clayton, R., Hafner, K., Cande, S., Raymond, C., 1999. Constraints on the proposed Marie Byrd Land – Bellingshausen plate boundary from seismic reflection data. Journal of Geophysical Research 104, 25,321 – 25,330.

Herzberg, C., Zhang, J., 1996. Melting experiments on anhydrous peridotite KLB-1: Compositions of magmas in the upper mantle and transition zone. Journal of Geophysical Research 101, 8271-8295.

Hirschman, M.M. and Stolper, E.M., 1996. A possible role for garnet pyroxenite in the origin of the “garnet signature” in MORB. Contributions to Mineralogy and Petrology 124, 185-208.

Hofmann, A.W., Jochum, K.P., Seufert, M., White, W.M., 1986. Nb and Pb in oceanic basalts: new constraints on mantle evolution. Earth and Planetary Science Letters 79, 33-45.

Hole, M.J., 1988. Post-subduction alkaline volcanism along the Antarctic Peninsula. Journal of the Geological Society of London 145, 985-998.

Hole, M.J., LeMasurier, W.E., 1994. Tectonic controls on the geochemical composition of Cenozoic mafic alkaline volcanic rocks from West Antarctica. Contributions to Mineralogy and Petrology 117, 187-202.

Larter, R.D., Cunningham, A.P., Barker, P.F., Gohl, K., Nitsche, F.O., 2002. Tectonic evolution of the Pacific margin of Antarctica, I. Late Cretaceous tectonic reconstructions. Journal of Geophysical Research 107 (B12), 2345, doi:10.1029/2000JB000052.

Lawver, L.A., Gahagan, L.M., 1994. Constraints on timing of extension in the Ross Sea region. Terra Antarctica 1, 545-552.

LeBas, M.J., LeMaitre, R.W., Streckeisen, A., Zanettin, B., 1986. A Chemical Classification of Volcanic Rocks Based on the Total Alkali-Silica Diagram. Journal of Petrology 27, 745-750

Leat, P.T., Thompson, M.A., Morrison, M.A., Hendry, G.L., and Dickin, A.P., 1988, Compositionally diverse, Miocene-Recent rift-related magmatism in Northwest Colorado: partial melting and mixing of mafic magmas from 3 different asthenospheric and lithospheric sources, in: Menzies, M.A., Cox, K.G. (Eds.) Oceanic and continental lithosphere. Journal of Petrology Special Lithosphere Issue pp. 331-349.

Lee, C.T.A., Luffi, P., Plank, T., Dalton, H., Leeman, W.P., 2009. Constraints on the depths and temperatures of basaltic magma generation on Earth and other terrestrial planets using

new thermobarometers for mafic magmas. Earth and Planetary Science Letters 279, 20-33.

LeMasurier, W.E., 2008. Neogene extension and basin deepening in the West Antarctic rift inferred from comparisons with the East African rift and other analogs. Geology 36, 247-250. doi: 10.1130/G24363A.1

LeMasurier, W.E., 2013. Shield volcanoes of Marie Byrd Land, West Antarctic rift: oceanic island similarities, continental signature, and tectonic controls. Bulletin of Volcanology 75, 726. doi: 10.1007/s00445-013-0726-1

LeMasurier, W.E., Landis, C.A., 1996. Mantle plume activity recorded by low relief erosion surfaces in West Antarctica and New Zealand. Geological Society of America Bulletin 108, 1450-1466

LeMasurier, W.E., Rex, D.C., 1989. Evolution of linear volcanic chains in Marie Byrd Land, West Antarctica. Journal of Geophysical Research 94, 7223-7236.

LeMasurier, W.E., Rex, D.C., 1990. Mt. Takahe, in: LeMasurier, W.E., Thomson, J.W. (Eds.) Volcanoes of the Antarctic Plate and Southern Oceans. American Geophysical Union, Antarctic Research Series 48, pp. 169-174.

LeMasurier, W.E., Thomson, J.W., (Eds.) 1990. Volcanoes of the Antarctic Plate and southern Oceans. American Geophysical Union, Antarctic Research Series 48, 487 p

LeMasurier, W.E., Harwood, D.M., Rex, D.C., 1994. Geology of Mt. Murphy volcano: an 8-m.y. history of interaction between a rift volcano and the West Antarctic ice sheet. Geological Society of America Bulletin 106, 265-280

LeMasurier, W.E., Futa, K., Hole, M.J., Kawachi, Y., 2003. Polybaric evolution of Phonolite, Trachyte and Rhyolite Volcanoes in Eastern Marie Byrd Land, Antarctica: controls on peralkalinity and silica saturation. International Geology Review 45, 1055-1099.

LeMasurier, W.E., Choi, S.H., Kawachi, Y., Mukasa, S.B., Rogers, N.W., 2011. Evolution of pantellerite-trachyte-phonolite volcanoes by fractional crystallization of basanite magma in a continental rift setting, Marie Byrd Land, Antarctica. Contributions to Mineralogy and Petrology 162, 1175-1199. doi: 10.1007/s00410-011-0646-z

Macdonald, G.A., Katsura, T., 1964. Chemical composition of Hawaiian lavas. Journal of Petrology 5, 82-133.

Marschall, H.R., Schumacher, J.C., 2012. Arc magmas sourced from mélange diapirs in subduction zones. Nature Geoscience 5, 862-867. Doi: 101038/NGEO1634

Martin, A.P., Cooper, A.F., Price, R.C., 2013. Petrogenesis of Cenozoic, alkali volcanic lineages at Mount Morning, West Antarctica and their entrained lithospheric mantle xenoliths: Lithospheric versus asthenospheric mantle sources. Geochimica et Cosmochimica Acta 122, 127-152. Doi: 10.1016/j.gca.2013.08.025

McDonough, W.F., Sun, S.S., 1995. The composition of the earth. Chemical Geology 120: 223-253

Mukasa, S.B., Dalziel, I.W.D., 2000. Marie Byrd Land, West Antarctica: evolution of Gondwana's Pacific margin constrained by zircon U-Pb geochronology and feldspar common-Pb isotopic compositions. Geological Society of America Bulletin 112, 611-629.

Mukasa, S.B., McCabe, R., Gill, J.B., 1987. Pb-isotopic compositions of volcanic rocks in the west and east Philippine island arcs: presence of the Dupal isotopic anomaly. Earth and Planetary Science Letters 84, 153-164.

Mukasa, S.B., Shervais, J.W., Wilshire, H.G., Nielson, J.E., 1991. Intrinsic Nd, Pb, and Sr isotopic heterogeneities exhibited by the Lherz alpine peridotite massif, French Pyrenees. Journal of Petrology Special Lherzolite Volume, pp. 117-134

Pankhurst, R.J., Weaver, S.D., Bradshaw, J.D., Storey, B.C., Ireland, T.R., 1998. Geochronology and geochemistry of pre-Jurassic superterranes in Marie Byrd Land, Antarctica. Journal of Geophysical Research 103, 2529-2547.

Panter, K.S., Hart, S.R., Kyle, P., Blusztajn, J., Wilch, T., 2000. Geochemistry of Late Cenozoic basalts from the Crary Mountains: characterization of mantle sources in Marie Byrd Land, Antarctica. Chemical Geology 165, 215-241

Pegram, W.J., 1990. Development of continental lithospheric mantle as reflected in the chemistry of the Mesozoic Appalachian Tholeiites, USA. Earth and Planetary Science Letters 97, 316-331.

Perinelli, C., Armienti, P., Dallai, L., 2011. Thermal Evolution of the Lithosphere in a Rift Environment as Inferred from the Geochemistry of Mantle Cumulates, Northern Victoria Land, Antarctica. Journal of Petrology 52, 665-690. Doi: 10.1093/petrology/egq099.

Peucker-Ehrenbrink, B., Hofmann, A.W., Hart, S.R., 1994. Hydrothermal lead transfer from mantle to continental crust: the role of metalliferous sediments. Earth and Planetary Science Letters 125, 129-142.

Plank, T., Langmuir, C.H., 1998. The chemical composition of subducting sediment and its consequences for the crust and mantle. Chemical Geology 145, 325-394.

Ritzwoller, M.H., Shapiro, N., Levshin, A.L., Leahy, G.M., 2001. Crustal and upper mantle structure beneath Antarctica and surrounding oceans. Journal of Geophysical Research 106, 30645-30670.

Rogers, N.W., 2006. Basaltic magmatism and the geodynamics of the East African rift system, in: Yirgu, G., Ebinger, C.J., Maguire, P.K.H. (Eds.) The Afar volcanic province within the East African rift system. Geological Society, London, Special Publications 259, pp. 77-93

Smellie, J.L., 2001. Lithofacies architecture and construction of volcanoes constructed in englacial lakes: Icefall Nunatak, Mount Murphy, eastern Marie Byrd Land, Antarctica, in: White, J.D.L., Riggs, N., (Eds.) Lacustrine volcaniclastic sedimentation. Special Publications of the International Association of Sedimentology, v30, pp. 9-34.

Stern, C.R., Frey, F.A., Futa, K., Zartman, R.E., Peng, Z., Kyser, T.K., 1990. Trace element and Sr, Nd, Pb, and O isotopic composition of Pliocene and Quaternary alkali basalts of the

Patagonian Plateau lavas of southernmost South America. Contributions to Mineralogy and Petrology 104, 294-308.

Todt, W., Cliff, R.A., Hanser, A., Hofmann, A.W., 1996. Evaluation of a ^{202}Pb-^{205}Pb double spike for high-precision lead isotope analysis, in: Basu, A., Hart, S.R. (Eds.) Earth Processes: Reading the Isotopic Code. Geophysical Monograph 95, pp. 429-437

Vogt, K., Gerya, T., 2014. Deep plate serpentinization triggers skinning of subducting slabs. Geology 42, 723-726. Doi: 10.1130/G35565.1

Weaver, B.L., 1991. The origin of ocean island basalt end-member compositions: trace element and isotopic constraints. Earth and Planetary Science Letters 104, 381-397

Wilch, T.I., McIntosh, W.C., Dunbar, N.W., 1999. Late Quaternary volcanic activity in Marie Byrd Land: potential $^{40}Ar/^{39}Ar$-dated time horizons in West Antarctic ice and marine cores. Geological Society of America Bulletin 111, 1563-1580.

Wilch, T.I., McCuddy, S.M., McIntosh, W.C., 2000. Middle and late Wisconsinan expansions of the West Antarctic ice sheet at Mt. Takahe volcano (abs), in: Volcano/ice interaction on Earth and Mars abstract volume. August 13-15, 2000. University of Iceland, Reykjavik, pp. 53.

Wilch, T.I., McIntosh, W.C., 2002. Lithofacies analysis and $^{40}Ar/^{39}Ar$ geochronology of ice-volcano interactions at Mt. Murphy and the Crary Mountains, Marie Byrd Land, Antarctica, in: Smellie, J.L., Chapman, M.G. (Eds.) Volcano-ice interaction on Earth and Mars. Geological Society Special Publication 202, London, pp 237-253

Wobbe, F., Gohl, K., Chambord, A., Sutherland, R., 2012. Structure and breakup history of the rifted margin of West Antarctica in relation to Cretaceous sparation from Zealandia and Bellingshausen plate motion. Geochemistry Geophysics Geosystems 13, 1-19. Doi: 10.1029/ 2011GC003742.

Wysoczanski, R.J., Gamble, J.A., Kyle, P.R., Thirlwall, M.F., 1995. The petrology of lower crustal xenoliths from the Executive Committee Range, Marie Byrd Land volcanic province, West Antarctica. Lithos 36, 185-201

Yakymchuk, C., Brown, C.R., Brown, M., Siddoway, C.S., Fanning, C.M., Korhonen, F.J., 2015. Paleozoic evolution of western Marie Byrd Land, Antarctica. Geological Society of America Bulletin 127, 1464-1484. doi: 10.1130/B31136.1

Zindler, A., Hart, S.R., 1986. Chemical geodynamics. Annual Reviews of Earth and Planetary Science 14, 493-571.

Figure captions.

Figure 1. Index map, subglacial topography, and inferred structure (cross-section) of the Marie Byrd Land dome and West Antarctic rift. The MBL dome is defined by contours on the low relief West Antarctic erosion surface (WAES) (LeMasurier and Landis, 1996). Structural relief on the dome from the inferred -500m base to crest (PT 2700) is ~ 3 km. Ice-free, isostatically adjusted bedrock topography is simplified from Drewry (1983). Abbreviations: *AR* Ames Range, *B* Mt. Bursey, *C* Mt. Cumming, *CM* Crary Mountains, *CN*

Coleman Nunatak, *E* Mt. Erebus, *ECR* Executive Committee Range, *F* Mt. Flint, *FR* Flood Range, *H* Mt. Hampton, *HB* Holmes Bluff, *HC* Hobbs Coast nunataks, *Hd* Hudson Mtns, *J* Jones Mtns, *M* Mt. Morning, *MBS* Marie Byrd Seamounts, *NVL* Northen Victoria Land, *P* Patton Bluff, *Pt* Mt. Petras, *RI* Ross Island, *SI* Shepard Island, *TAM* Transantarctic Mountains, *Tn* Toney Mountain, *VL* Victoria Land. Greenwich meridian is up, following the convention for small scale maps of Antarctica.

Figure 2. A plate tectonic and geologic reconstruction showing inferred spatial and geologic relationships between West Antarctica and Zealandia in pre-85 Ma time, modified from Cooper et al., (1982). Positions of the convergent plate margin and Pacific-Phoenix Ridge at ca. 105 Ma are adapted from Lawver and Gahagan (1994). The continuity of the Cretaceous plutonic belt and the Torlesse belt shows the overall geologic integrity of the reconstruction. West Antarctic erosion surface (WAES) data are from LeMasurier and Landis (1996). Abbreviations. *AI* Alexander Island, *Ak* Auckland city, *CI* Campbell Island, *C* Canterbury, *Ch* Chatham Islands, *F* Fiordland, *HC* Hobbs Coast nunataks, *J* Jones Mountains, *O* Otago, *P* Pacific-Phoenix Ridge, *STR* South Tasman Rise, *Tas* Tasmania, *TI* Thurston Island.

Figure 3. Geologic sketch map of Mt. Murphy, modified from LeMasurier and Thomson (1990, p.165) and Smellie (2001), showing numbered sample localities and $^{40}Ar/^{39}Ar$ ages from Wilch and McIntosh (2002). Sample numbers shown in Table 1 include year collected, numbered sample locality, and letters to distinguish between multiple samples collected

from the same locality, e.g. for sample number 85-32B: 85=year collected, 32=sample locality shown on this figure, B=one of several samples collected at this locality.

Figure 4. Geologic sketch map of Mt. Takahe (LeMasurier and Thomson, 1990, p. 170) showing numbered sample localities, and isotopic ages from Wilch et al., (2000). Sample numbers shown in Table 1 include year collected, numbered sample locality, and letters to distinguish multiple samples from the same locality, as in Fig. 3.

Figure 5. (A) IUGS classification of Mt. Takahe – Mt. Murphy – Mt. Siple basaltic rocks based on the total alkalies – silica (TAS) diagram (Le Bas et al., 1986). (B) TAS diagram including basaltic rocks from panel (A), plus basaltic samples from 15 other MBL volcanic centers (the "comparative suite"). **Red circles**, Mt. Takahe; **blue squares**, Mt. Murphy basal succession; **red squares**, Mt. Murphy parasitic cones; **blue triangle**, Mt. Siple basal succession; **red triangle**, Mt. Siple parasitic cone; **"X"**, Comparative suite: Ames/Flood Ranges, 4 volcanoes (LeMasurier et al., 2011); Hobbs Coast, 4 nunataks (Hart et el., 1997); Executive Committee Range, 3 volcanoes (LeMasurier et al., 2003); Mt. Flint, Mt. Petras, Shepard Island (LeMasurier and Thomson, 1990); Crary Mountains (Panter et al., 2000). See Fig. 1 for all locations. **M-K (1964)** is the boundary between tholeiitic and alkali basalts of Macdonald and Katsura (1964). Major elements recalculated to 100%, volatile free, following LeBas et al., (1986).

Figure 6. Major element variation diagrams for Mt. Takahe, Mt. Murphy, Mt. Siple, plus comparative suite. **a.** MgO vs Na_2O **b.** MgO vs Ni **c.** MgO vs CaO **d.** CaO/Na_2O vs V (Hart et al., 1997).

Figure 7. Multi-element plot of two Mt. Takahe and three Mt. Murphy basaltic rocks normalized to primordial mantle (McDonough and Sun, 1995). Included for comparison are basanites from the Ames Range (LeMasurier et al., 2011) and Jones Mountains (Hart et al., 1995).

Figure 8. Selected trace element plots of Mt. Takahe-Mt. Murphy-Mt. Siple basaltic rocks, compared with the comparative suite plus Jones Mountains (Hart et al. 1995). Vertical dashed lines on plots A, B, D, and F, roughly separate Hobbs Coast and Ames/Flood Range basalts in the west (see Fig 1) from Mt. Takahe, Mt. Murphy, and the Jones Mountains basalts in the east, to help illustrate the west to east Nb gradient. Clusters of most samples from Mt. Murphy, Mt. Takahe, Hobbs Coast, and AR/FR are encircled, where it can be done without adding clutter, to help visualize patterns described in the text. (A**)** Nb versus Ba. (**B)** Nb versus K. **(C)** K versus Ba/La **(D)** Ba/Nb versus K/Nb. HIMU and EM1 average end member points, here and in Fig. 8E, are from Hart and Gaetani (2006). The shaded area labeled AP is the range for Antarctic Peninsula basalts. AP and Hudson Mountains range are from Hole and LeMasurier (1994). **(E)** Ba/La versus Ba/Nb. (**F)** Nb versus Ta. Only ICPMS data are used for diagrams that involve La. The encircled samples are Mt. Murphy (M, in blue), Mt. Takahe (T, in red), Hobbs Coast (HC, in black), Ames and Flood Ranges (AR/FR, dotted line).

Figure 9. **a.** Pb/Ce versus Ba/Nb. **b.** Nb versus Th/Pb. **C.** Nb versus Nb/Y. Only ICPMS data are used for diagrams that involve Ce, Pb, and Th. OIB end members EM1, and HIMU are from Hart and Gaetani (2006). GLOSS is from Plank and Langmuir (1998). Encircled

samples are Mt. Murphy (M, in blue), Mt. Takahe (T, in red), and Jones Mountains (J, in green).

Figure 10. **a.** $^{143}Nd/^{144}Nd$ versus $(^{87}Sr/^{86}Sr)_I$ isotopic ratios for Mt. Takahe, Mt. Murphy and Mt. Siple. The field "MBL basaltic rocks," includes all available data from elsewhere in the province, from Futa and LeMasurier (1983); Hole and LeMasurier (1994); Hart et al., (1997); Panter et al., (2000). Jones Mountains points are from Hart et al., (1995). Fields for mid-ocean ridge basalts (MORB) and mantle components are from Zindler and Hart (1986): EM1 and EM2 enriched mantle of type 1 and 2 respectively, HIMU mantle with high U/Pb ratio. HIMU, EM1 and EM2 end member points are from Hart and Gaetani (2006). BSE is bulk silicate earth. Field for potential lower crustal contaminants is from Futa and LeMasurier, (1983), and Wysoczanski et al., (1995); the field for MBL upper crustal granitoids and gneisses is from Pankhurst et al., (1998); data for peridotite xenoliths from West Antarctica are from Martin et el., (2013), and for pyroxenite xenoliths from Wysoczanski et al., (1995); Perinelli et el., (2011); Martin et el., (2013). Error bars are 2σ, given only where they exceed the size of the symbol in the plot.

b. La/Nb versus $^{143}Nd/^{144}Nd$, modified from Hole and LeMasurier (1994), and showing the range of basalt compositions in West Antarctica, compared with western U.S. (Leat et al., 1988; Fitton et al., 1988).

c. $^{143}Nd/^{144}Nd$ versus $(^{87}Sr/^{86}Sr)_i$ for Mt. Takahe, Mt. Murphy, and Mt. Siple basaltic rocks plus those from the comparative suite. Locations for all samples can be found in Fig. 1. Encircled samples as in Fig. 8.

Figure 11. $^{208}Pb/^{204}Pb$ versus $^{206}Pb/^{204}Pb$, and $^{207}Pb/^{204}Pb$ versus $^{206}Pb/^{204}Pb$, for Mt. Takahe, Mt. Murphy and Mt. Siple. Also shown are available Pb data for MBL lower crustal rocks (Wysoczanski et al., 1995), MBL granitoids and gneisses (Mukasa and Dalziel, 2000), and basaltic rocks from elsewhere in the MBL province (Hart et al., 1997; Panter et al., 2000) plus Jones Mountains (Hart et al., 1995), and peridotite and pyroxenite xenoliths from West Antarctica (Wysoczanski et al., 1995; Martin et al., 2013). Fields for oceanic basalts and mantle components are from Zindler and Hart (1986). EM1 and EM2 enriched mantle of type 1 and 2, respectively, HIMU mantle with high U/Pb ratio. MORB mid-ocean ridge basalts. HIMU, EM1, and EM2 end member points are from Hart and Gaetani (2006). NHRL is the Northern Hemisphere Reference Line of Hart (1984). Error bars are 2σ, given only where they exceed the size of the symbol in the plot.

Figure 12. Multi-element plot of high-Ba (85-32B, 67-66B) and low-Ba (67-62; 85-19) basaltic rocks from Mt. Murphy and Mt. Takahe, respectively. Also included are Ames Range sample AR60E, GLOSS (Plank and Langmuir, 1998) and Avg EM1 (Hart and Gaetani, 2006), all normalized to primitive mantle (McDonough and Sun, 1995).

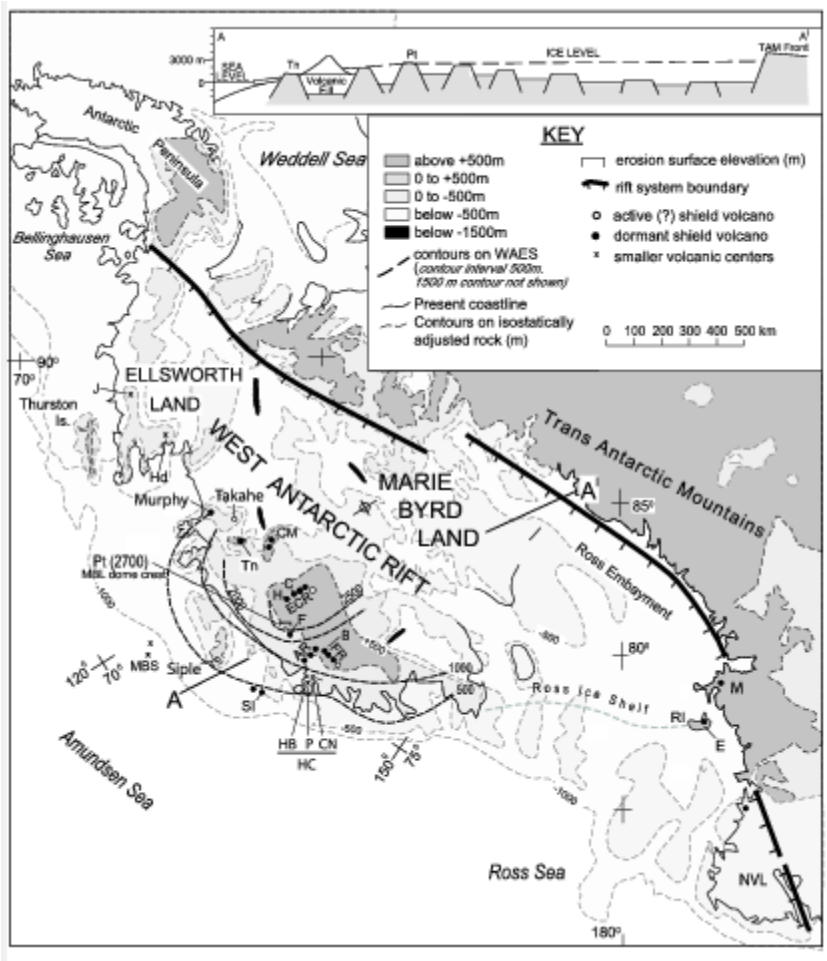

Figure 1

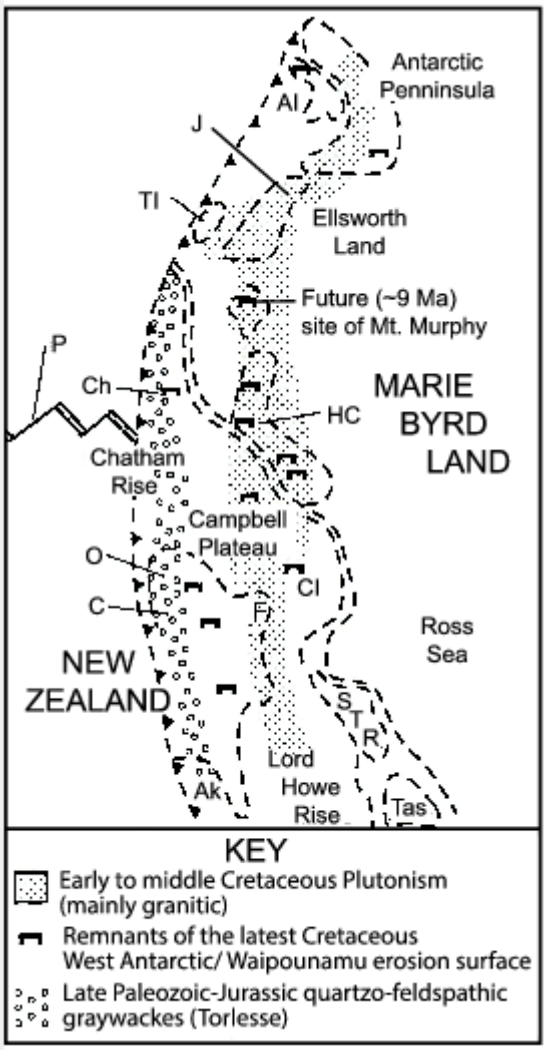

Figure 2

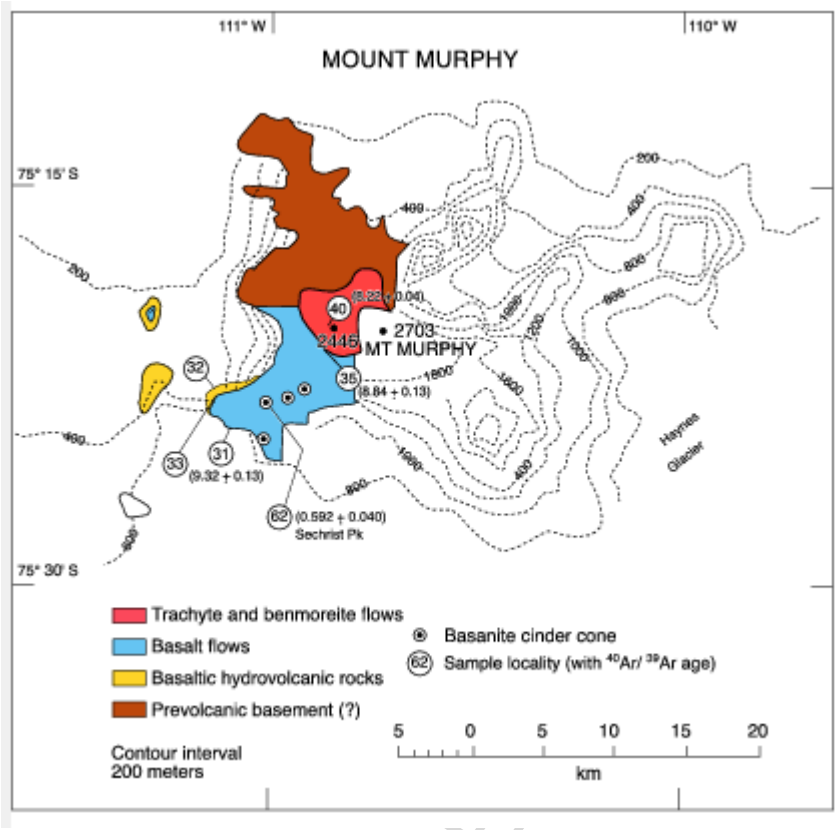

Figure 3

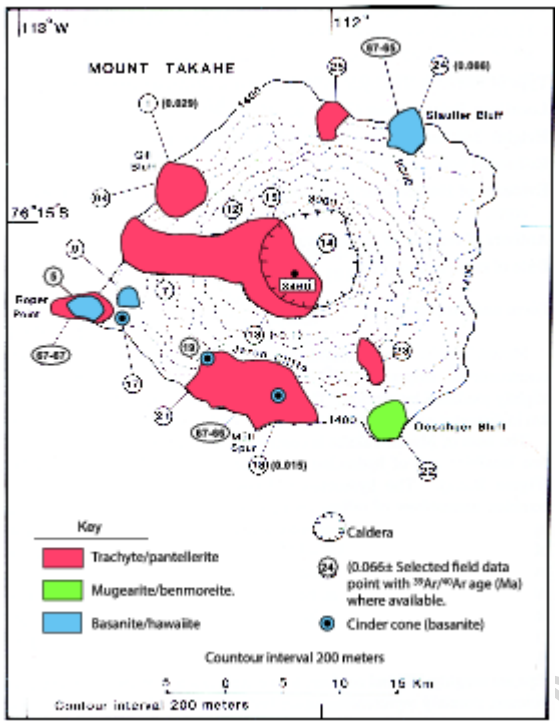

Figure 4

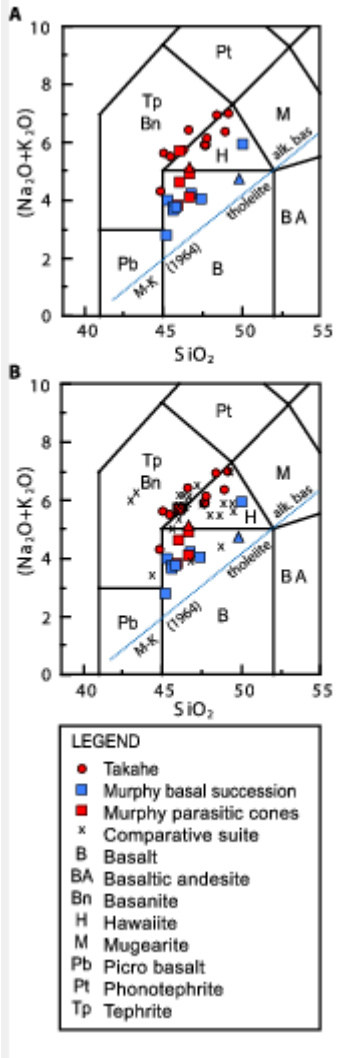

Figure 5

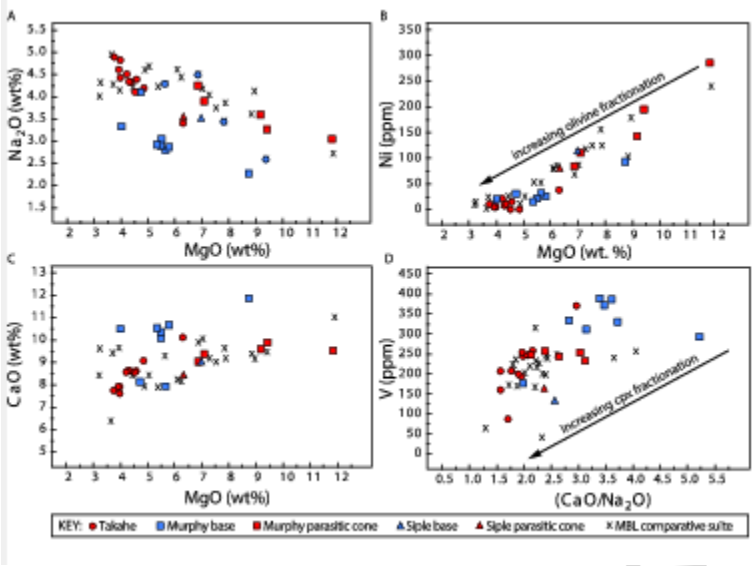

Figure 6

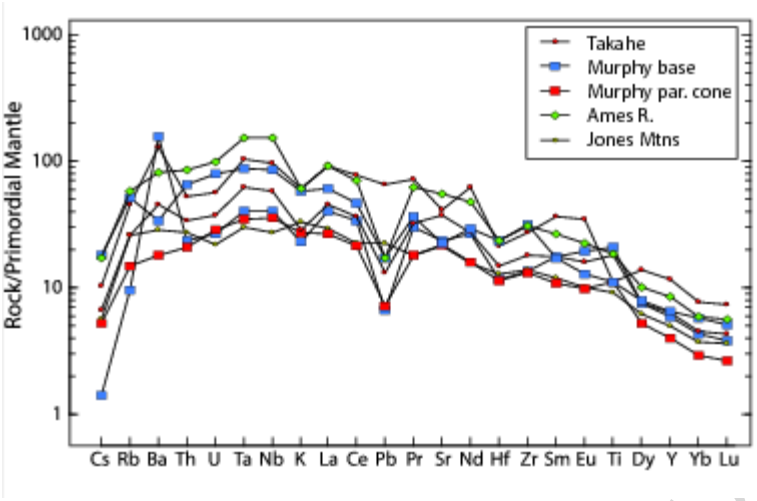

Figure 7

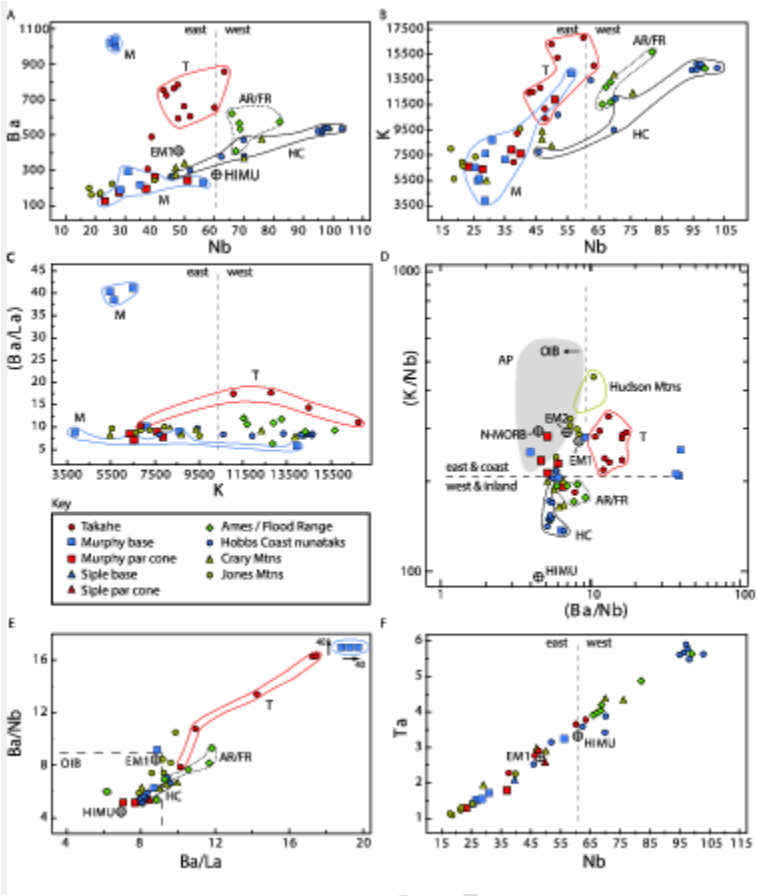

Figure 8

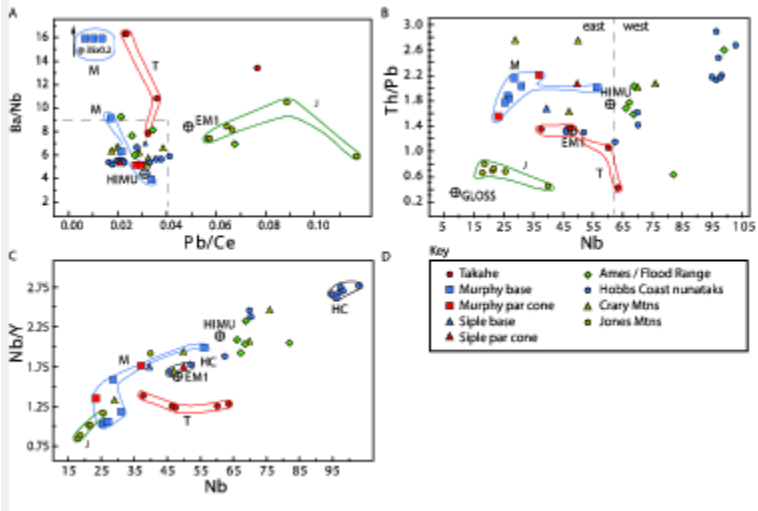

Figure 9

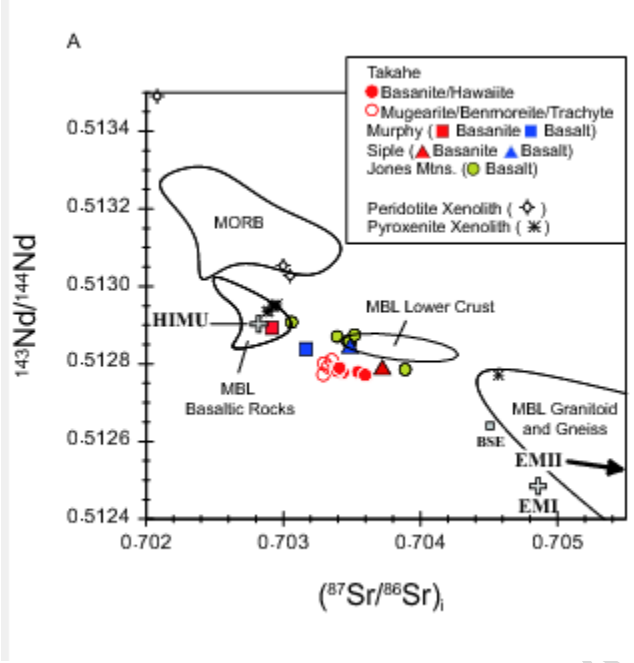

Figure 10a

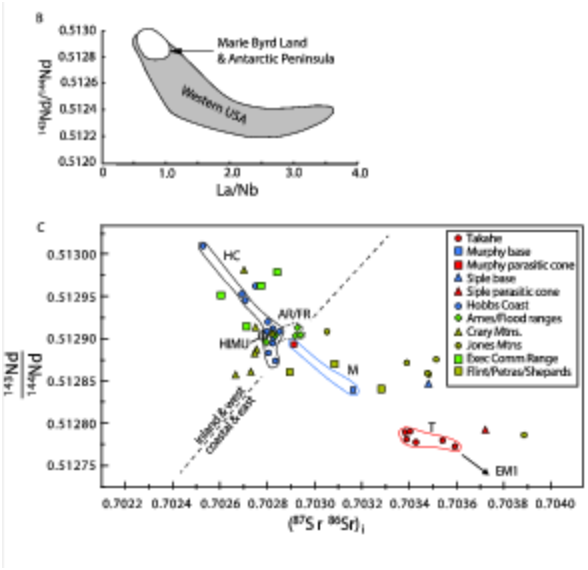

Figure 10b

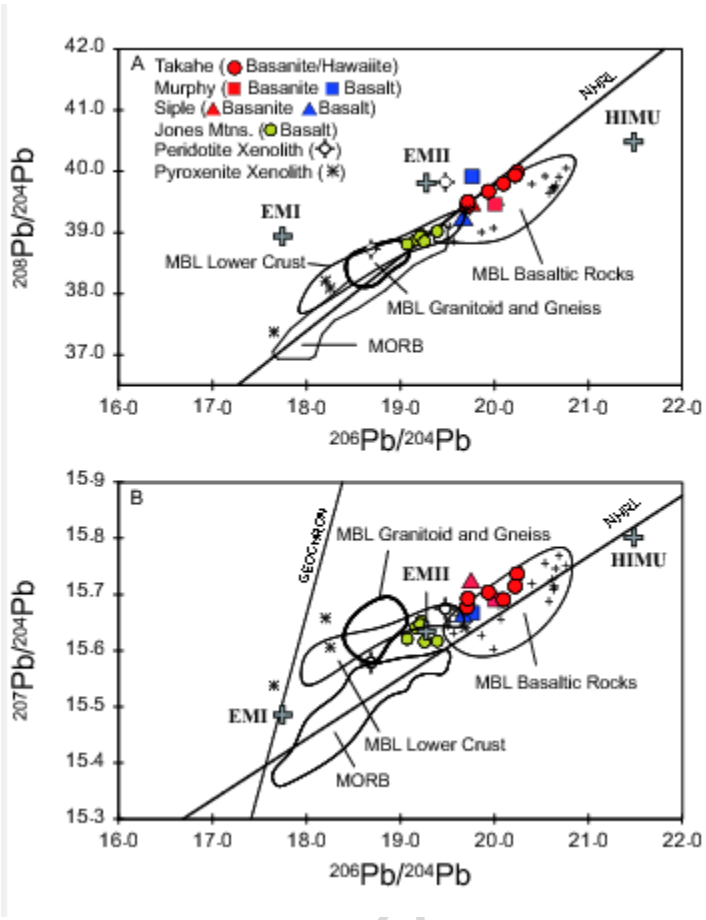

Figure 11

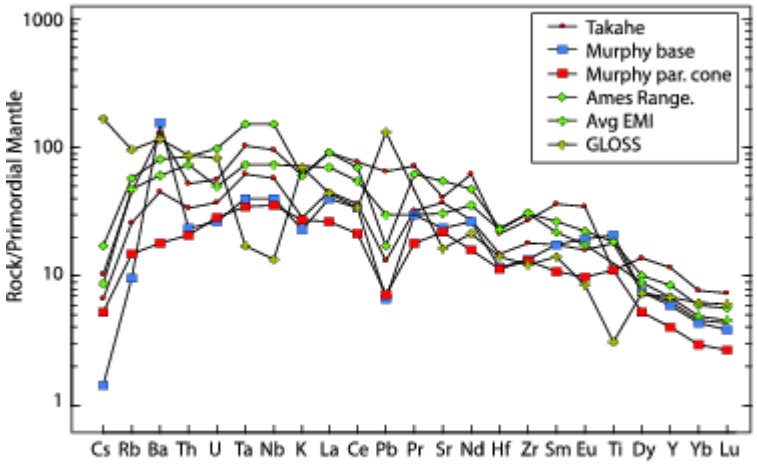

Figure 12

Table 1. Chemical Data for Mt. Takahe, Mt. Murphy, and Mt. Siple basaltic rocks. hInterlab Comparisons

	Takahe												**Siple**	**Siple**			**Murphy**															
																								Sechrist P	Sechrist P	800m	2446m						
Locality	Roper Pt	Roper Pt	Roper Pt	Roper Pt	Steuri gl	Jaron Cl	Staufer Bl	Staufer Bl	Staufer Bl	Staufer Bl	duplicate	basal sec	parcone	Locality	Warm, S	Warm, N	Warm, N	Warm, N	Warm	Warm	till it e site	parcone	parcone	parcone	parcone	parcone						
Rock type	hawaiite	hawaiite	basanite	basanite	basanite	basanite	hawaiite	hawaiite	hawaiite	basanite	trace s	subalkali	alkali	Rock type	alkali	alkali	subalkali	subalkali	alkali	subalkali	alkali	alkali	alkali	alkali	alkali	alkali	Open	Open	Open	Göttingen	Göttingen	Göttingen
												basalt	basalt		basalt	basalt	basalt	basalt	basalt	basalt	basalt	basalt	basalt	basalt	basalt	basalt	University	University	University	University	University	University
Ar-							0.0							Ar-																		

Arage (m.y.)a							66±4.7							Arage																
Ar-Arage (m.y.)b														Ar-Arage							8.84±0.13		0.592±0.04							
																									Recom	.Meas.	St.Dev	Recom	MeasAvg	St.Dev
Samplenumber	85-5C3	85-5E1	67-67A	85-17C	85-19	67-66B	85-24D	85-24B	85-24C	67-65B	67-65B	W83-5Cef	W83-1ef	Sample#	85-31Ad	85-32Ed	85-32Gd	85-32Bdf	85-33Fd	85-33Bd	85-35Bc	85-34c	67-62df	85-38c	85-39c	85-40Ed	JB-2	JB-2	JB-2	JA-2	JA-2	JA-2
SiO2	48.48	48.64	48.51	45.16	44.62		47.34	47.41	47.54	47.12		48.98	45.46	SiO2	49.00	44.47	45.08	45.13	44.41	44.96	46.42	45.83	46.19	46.26	46.01	45.69						
TiO2	3.14	3.28	3.28	4.43	3.66		3.53	3.50	3.46	3.56		1.77	3.21	TiO2	2.24	3.58	4.16	4.20	2.56	4.07	4.28	2.94	2.22	2.61	3.08	2.56						
Al2	14.	14.	14.	14.	15.		15.	15.	15.	15.		14.	15.	Al2	16	14.	13.	13.	15	13.	16.	15	13.7	13.	14	14						

O3	44	50	85	18	26		22	18	19	52		74	15	O3	.50	51	69	62	.20	86	12	.26	6	89	.51	.55						
Fe2O3	3.37	2.72		2.57	4.41		2.23	2.55	2.48			1.54	1.28	Fe2O3	4.60	4.57	4.43	3.81	3.87	5.01	3.15	3.74	2.91	1.72	3.45	2.96						
FeO	9.18	10.31	12.75	11.51	9.79		10.60	10.28	10.29	12.90		9.43	11.67	FeO	6.04	9.00	10.64	11.24	8.07	9.79	9.82	9.02	9.60	10.49	9.25	9.56						
MnO	0.29	0.28	0.29	0.26	0.21		0.25	0.27	0.26	0.25		0.18	0.19	MnO	0.18	0.23	0.26	0.26	0.18	0.24	0.20	0.23	0.15	0.20	0.21	0.18						
MgO	3.78	3.99	3.94	4.87	6.34		4.31	4.37	4.25	4.30		7.00	6.34	MgO	4.74	5.82	5.36	5.50	8.75	5.52	4.02	6.89	11.87	9.44	7.11	9.20						
CaO	7.71	7.88	7.89	9.06	10.10		8.57	8.59	8.55	8.74		9.03	8.42	CaO	8.12	10.64	10.53	10.35	11.86	10.09	10.49	9.02	9.53	9.90	9.35	9.57						
Na2O	4.88	4.41	4.54	4.18	3.40		4.33	4.31	4.49	4.37		3.51	3.54	Na2O	4.09	2.86	2.91	3.05	2.27	2.90	3.33	4.24	3.04	3.26	3.90	3.60						
K2O	1.96	1.83	1.99	1.25	0.83		1.49	1.50	1.54	1.55		1.13	1.42	K2O	1.68	1.04	0.68	0.66	0.47	0.78	0.86	1.43	0.79	0.77	0.92	0.95						
P2O5	1.27	1.35	1.38	1.66	0.62		1.21	1.24	1.20	1.34		0.91	0.71	P2O5	0.70	1.27	0.96	0.95	0.51	0.91	0.49	0.82	0.42	0.42	0.67	0.44						
H2O	0	0	0.00	0	0		0	0	0	0.00		0.00	0.00	H2O	0.0	0.00	0.00	0.00	0.0	0.00	0.00	0.0	0.20	0.00	0.0	0.0						

+															+	0				0			0			0	0						
H2O-	0.05	0.00	0.00	0.00	0.00		0.00	0.00	0.00	0.00		0.00	0.00	H2O-	1.42	1.43	0.39	0.18	1.26	1.11	0.00	0.00	0.00	0.00	0.00	0.00						
F	0.09	0.09	0.00	0.12	0.05		0.08	0.10	0.08	0.00		0.06	0.09	F	0.04	0.06	0.05	0.06	0.03	0.05	0.03	0.05	0.03	0.03	0.02	0.03						
CO2	0	0	0	0	0		0	0	0	0		0	0	CO2	0	0	0	0	0	0	0	0	0	0	0	0						
															-	-	-	-	-	-	-	-	-	-	-	-						
Total	98.64	99.28	99.43	99.25	99.29		99.16	99.30	99.33	99.63		98.28	97.48	Total	99.35	99.48	99.14	99.01	99.44	99.29	99.21	99.47	100.71	98.99	98.48	99.29						
-	-	-	-	-	-	-	-	-	-	-				-	-	-	-	-		-	-	-	-	-	-	-						
Li			8.91		5.03	7.53			5.75	5.77	5.67	5.73	7.00	Li	8.36	4.40	4.74	3.30	4.06	3.75			4.96			5.84	8.08	8.36	0.17	27.30	29.98	0.71
Sc			21.6		29.4	21.1			21.3	22.5	21.5	25.57	25.9	Sc	20.45	27.17	34.06	33.55	29.23	32.43			25.99			26.04	54.08	54.24	1.04	19.60	22.11	0.36
Ti			201777		224311	194000			205800	212296	207881			Ti	-	-	-	-	-	-	-	-	-	-	-	-	69960	68970	1420			
V	205	206	159	256	369	85	252	243	197	192	189	132	163.00	V	176	330	386	388	291	371	310	246	231	252	256	242	5724	574	5.22			
Cr	9	7	4.	6	2	8.	1	1	1	8.	8.	2	1	C	6	3	2	2	1	3	3	1	51	3	2	2	2	2	0.			

			39		4	25	2	7	4.6	41	24	77	02	r	3	3	8	5	70	0	3	75	4	37	50	85	6.65	7.38	37			
Co	26.0	27.0	29.5	31.0	52.6	19.8	35.0	39.0	30.4	30.8	30.0	34.67	40.91	Co	28.89	39.06	46.04	44.84	48.75	44.21	36	43	53.54	54	44	49.96	37.57	37.69	1.6	29.50	30.09	0.92
Ni	9.0	4.0	6.9	0.0	37.4	3.4	7.0	9.0	19.2	13.9	13.7	102.8	71.5	Ni	31.7	25.5	23.7	22.6	92.4	23.5	20	84	250.6	195	110	139.6	14.77	13.88	0.22	130.00	132.79	2.94
Cu	34	8	22.6	26	53.2	6.81	8	28	21.2	20.3	19.8	29.75	37.22	Cu	36.90	41.77	61.83	59.87	57.03	58.76	63	54	58.87	68	54	56.62	2221	214	1.84	29.70	26.34	0.61
Zn	139	137	147	112	108	137	113	109	115	120	119	100.1	121.6	Zn	98.4	103.7	120.4	118.0	85.4	115.8	87	94	102.1	93	102	90.3	110.4	110	1.20	64.70	66.19	1.63
Ga	22.0	21.0	26.6	20.0	22.7	25.9	23.0	20.0	24.1	24.8	25.0	21.0	22.0	Ga	22	18	19	21.0	18	19	24	20		19	19	18	16.62	16.22	0.153			
Rb	32.0	29.0	32.2	20.0	15.4	26.9	23.0	20.0	19.9	18.8	18.5	19.99	24.10	Rb	30.87	9	5.75	5.78	6.46	5.11	17	19	8.93	14	15	14	6.4	6.32	0.0066	72.90	70.99	0.69
Sr	593	600	607	793	750	816	747	748	750	785	780	423.1	454.5	Sr	449.4	890.1	469.0	469.8	578.8	454.0	580	904	435.6	622	872	434.1	178.2	176.70	1.63	248.00	242.28	1.49
Y	43.0	45.0	48.7	40.0	27.6	50.0	37.0	36.0	37.3	39.2	38.9	22.79	28.65	Y	28.2	26.35	25.55	25.32	18.2	24.91	24	32	17.49	23	27	21.2	23.56	24.87	0.093	18.30	16.77	0.17

															6				0							0						
Zr	243	249	290	214	192	286	197	193	206	214	211	187.0	241.5	Zr	327.2	143.1	143.7	140.7	124.4	133.3	161	229	139.9	153	187	179.3	48.25	47.44	0.403	116.00	120.53	0.99
Nb	50.0	52.0	60.3	48.0	37.8	63.6	43.0	44.0	46.5	47.8	47.5	39.72	49.88	Nb	56.29	31.03	26.94	26.54	28.70	25.57	35	51	23.45	28	40	37.23	0.5565	0.551	0.0005	9.47	9.28	0.004
Sn			1.94		1.71	0.77			0.59	1.77	1.75	1.38	1.77	Sn	2.55	1.05	1.19	1.18	1.02	1.12			1.24			1.44	0.6635	0.554	0.228	1.68	1.67	0.004
Sb			0.06		0.05	0.07			0.04	0.04	0.03	0.04	0.03	Sb	0.11	0.04	0.03	0.03	0.03	0.03			0.03			0.04	0.2611	0.223	0.0111	0.114	0.115	0.001
Cs			0.28		0.14	0.22			0.14	0.14	0.14	0.21	0.18	Cs	0.38	0.12	0.03	0.03	0.07	0.06			0.11			0.23	0.8	0.822	0.0015	4.663	4.800	0.008
Ba	657	597	648	585	296	851	746	718	758	776	784	276.8	267.3	Ba	221.3	283.6	998.9	1034.5	1801.2	1019.9	211	236	120.7	168	258	1911.2	2181.1	223	4.13	321.00	296.60	4.57
La			59.0		29.1	59.5			43.3	44.9	44.7	29.04	31.46	La	38.87	32	26.02	25.72	200.58	24.82	21	52	17.09	20	29	24.82	2.2281	2.226	0.0026	15.880	15.880	0.18
Ce			125		61.1	128			92.8	96.1	95.9	57.53	65.12	Ce	77.14	68.69	57.04	56.39	43.61	54.52	62	83	36.13	61	68	50.68	6.552	6.52	0.0073	32.70	32.30	0.29
Pr			17.		8.2	18.			13.	14.	14.	7.0	8.3	Pr	9.	9.0	7.7	7.6	5.	7.3			4.64			6.	1.1	1.1	0.0	3.8	3.7	0.0

			6			4			3	0	0	3	0		32	1	5	3	57	3						26	29	5	13	4	4	5
Nd			72.7		34.0	76.9			54.7	58.1	57.5	28.12	33.92	Nd	36.38	38.53	33.52	33.55	23.67	32.26			19.86			25.06	6.392	6.31	0.093	13.90	14.25	0.18
Sm			14.1		7.11	14.8			10.9	11.4	11.4	5.77	7.08	Sm	6.98	7.78	7.23	7.10	4.92	6.90			4.45			5.29	2.266	2.29	0.036	3.11	3.02	0.10
Eu			4.26		2.47	5.37			4.24	4.46	4.43	1.91	2.22	Eu	2.00	2.69	3.05	3.02	1.71	2.90			1.52			1.67	0.8336	0.8333	0.0013	0.93	0.89	0.002
Gd			12.6		6.66	13.3			9.88	10.4	10.3	5.38	6.69	Gd	6.46	7.15	6.85	6.78	4.71	6.57			4.31			5.03	3.1123	3.16	0.0084	3.06	3.02	0.008
Tb			1.76		0.95	1.83			1.36	1.43	1.42	0.76	0.95	Tb	0.91	0.95	0.92	0.91	0.63	0.89			0.62			0.71	0.586	0.602	0.0005	0.44	0.47	0.001
Dy			9.15		5.07	9.42			7.03	7.35	7.30	4.41	5.52	Dy	5.36	5.25	5.14	5.13	3.60	4.92			3.54			4.12	3.868	3.94	0.0054	2.80	2.88	0.004
Ho			1.76		0.98	1.79			1.34	1.39	1.37	0.82	1.04	Ho	1.02	0.97	0.94	0.94	0.66	0.91			0.64			0.79	0.863	0.899	0.0009	0.50	0.60	0.001
Er			4.41		2.49	4.47			3.29	3.45	3.41	2.23	2.78	Er	2.83	2.51	2.44	2.44	1.74	2.38			1.67			2.09	2.537	2.61	0.0021	1.48	1.70	0.003
Yb			3.42		2.00	3.43			2.52	2.61	2.59	1.86	2.37	Yb	2.53	1.99	1.96	1.92	1.43	1.87			1.30			1.80	2.529	2.53	0.0026	1.62	1.65	0.004

Lu			0.50		0.29	0.50			0.36	0.38	0.37	0.25	0.32	Lu	0.35	0.27	0.26	0.26	0.19	0.25			0.18			0.26	0.38944	0.3833	0.0006	0.27	0.24	0.001
Hf			6.20		4.20	6.02			4.47	4.63	4.60	4.03	5.29	Hf	6.71	3.28	3.39	3.34	2.89	3.25			3.22			3.97	1.4887	1.45	0.0019	2.86	3.02	0.006
Ta			3.63		2.27	3.77			2.76	2.89	2.83	2.08	2.58	Ta	3.24	1.72	1.52	1.50	1.55	1.41			1.28			1.79	0.03996	0.0048	0.0008	0.80	0.061	0.001
Pb			4.51		1.99	9.86			2.21	2.24	2.22	1.80	1.38	Pb	2.60	1.19	1.02	1.00	0.95	1.01			1.07			1.39	5.25	5.16	0.1533	19.200	17.003	0.200
Th			4.73		2.67	4.12			2.95	3.02	2.96	3.00	2.84	Th	5.22	2.41	1.86	1.87	2.05	1.79			1.65			3.06	0.255776	0.27	0.0002	5.03	5.03	0.005
U			1.24		0.75	1.15			0.76	0.73	0.73	0.81	0.72	U	1.62	0.67	0.53	0.54	0.83	0.42			0.58			0.99	0.152828	0.15	0.0004	2.21	2.27	0.004
Sr87/86i			0.703546	0.703386	0.703434					0.703395		0.703487	0.703723	Sr87/86i	-	-	-	0.703165	-	-			0.702917	-	-	-						
Nd143/			0.5112	0.5112	0.5112					0.5112		0.5112	0.5112	Nd14				0.5112					0.512893									

144			780	789	778					781		847	792	3/144				839													
Pb206/204			19.706	20.243						19.937		19.669	19.753	Pb206/204				20.010					19.764								
Pb207/204			15.677	15.737						15.704		15.665	15.725	Pb207/204				15.691					15.667								
Pb208/204			39.422	39.993						39.675		39.251	39.494	Pb208/204				39.463					39.195								
Mg Number	0.42	0.43	0.43	0.46	0.52		0.45	0.45	0.45	0.45				Mg#	0.53	0.51	0.47	0.47	0.64	0.48	0.43	0.57	0.70	0.65	0.58	0.64					
%normative	0.00	0.00	0.00	0.00	0.00		0.00	0.00	0.00	0.00		3.34	0.00	%hy	0.00	0.00	1.99	0.17	0.00	2.26	0.00	0.00	0.00	0.00	0.00	0.00					

hyg																														
%normative ol	12.22	13.70	16.11	14.55	16.78		11.70	13.61	13.05	13.85		15.89	18.42	%ol	14.04	15.81	13.54	15.14	19.15	14.10	10.31	17.43	26.25	20.79	17.22	21.02				
%normative ne	5.38	2.11	4.69	4.43	5.00		3.76	3.58	4.65	4.64		0.00	3.68	%ne	1.87	1.04	0.000	0.000	1.88	0.00	1.05	9.07	4.37	4.05	5.65	7.02				

[a]Wilch et el. (2000)

[b]Wilch et al. (2002)

[c]LeMasurier (2013)

[d]LeMasurier (2013)

[e]LeMasurier and Thomson (1990) major elements only

[f]Hart et al. (1997) isotopes only

[g]norms calculated volatile free with Fe2O3 = 0.1 (FeO total)

[h]Recom = recommended; Meas = measured; St. Dev. = standard deviation major elements only

TABLE 2. Ranges of incompatible trace element ratios in MBL basalts compared to OIB averages (Hart and Gaetani, 2006)

	Takahe	Murphy	**AR/FR**	**ECR**	**Hobbs Cst**	**HIMU**	**EM1**	**EM2**
Ba/Th	110-257*	42.4 - 570	70-152	58.9-162	88-92	63.2	68.4	53.7
Ba/Nb	7.8-16.3	4.0 - 40	5.7-9.3	5.7-8.4	5.1-5.7	4.48	8.38	6.43
Ba/La	10.2-17.5	5.7-41.1	6.2-11.9	7.2-11.4	8.2-8.4	6.89	8.83	6.93
K/Nb	182-278	135-280	145-193	168-234	139-213	103	274	282

*** Red numbers are outside normal OIB ranges.**

Highlights

- Three MBL volcanoes display Ba and Nd isotope anomalies unique to West Antarctica
- Neither lithospheric contamination, nor mantle amphibole explains the anomalies
- Residual subduction component contamination provides the best explanation
- Subduction ended ~85 Ma followed by formation of the West Antarctic rift
- The anomaly source is a fossil mantle diapir attached to the base of the lithosphere